

SUPPORTING INFORMATION

Ruthenium(II) complexes of pyridinol and N-heterocyclic carbene derived pincers as robust catalysts for selective carbon dioxide reduction

Chance M. Boudreaux,^{†,a} Nalaka P. Liyanage,^{†,b} Hunter Shirley,^b Sopheavy Siek,^a Deidra L. Gerlach,^a Fengrui Qu,^a Jared H. Delcamp,^{*,b} Elizabeth T. Papish^{*,a}

^aUniversity of Alabama Department of Chemistry, Tuscaloosa, AL 35487, USA

^bUniversity of Mississippi, Department of Chemistry and Biochemistry, Coulter Hall, University, MS 38677, USA

[†]Authors contributed equally

*Corresponding authors. Email: delcamp@olemiss.edu & etpapish@ua.edu

Table of Contents

General Methods	S3
Photocatalysis General Information	S3
Photocatalysis Procedure	S3
Synthesis of Compounds and Complexes	S4-6
Spectral Data	S7-35
2,6-di(1H-imidazol-1-yl)-4-methoxypyridine (6)	S7-11
1,1'-(2,6-p-methoxypyridinediyl)bis[3-methyl-1H-Imidazolium] ditriflate (7)	S12-16
[Ru(CNC-OMe)(ACN)₂Cl]OTf (2)	S16-23
[Ru(CNC-OMe)(ACN)₃](OTf)₂ (3)	S24-30
[Ru(CNC-H)(ACN)₂Cl]OTf (4)	S31-35
UV-Vis spectra for the catalysts (Figure S30)	S36
CVs of catalysts 1-4 in MeCN (Figure S31)	S37
Thermodynamic Figure Discussion	S37
An illustration of a photocatalytic CO₂ reduction	S38
¹H NMR Formate Detection	S38-41
Comparison and Discussion on Known Ruthenium Catalysts for CO₂	
Photoreduction	S42-44
XRD Structure Determinations	S45-46
References	S47

General Methods. All syntheses were performed as reported in the manuscript. All solvents were dried on a glass contour solvent purification system built by Pure Process Technology, LLC or were used through commercially available dry solvents. Other commercially available reagents were used without further purification necessary. All reactions were prepared and executed under an inert N_{2(g)} environment utilizing Schlenk line techniques or glovebox and oven or flame dried flask. Purifications were conducted open to air unless otherwise stated. Literature procedures were used for the preparation of 2,6-difluoro-4-methoxypyridine and 1,1'-(2,6-pyridinediyl)bis[3-methyl-1H-Imidazolium] ditriflate.¹⁻² NMR spectra were collected utilizing a Bruker AV360 360 MHz or AV500 500 MHz NMR spectrophotometer. Mid-IR spectra were obtained utilizing a Bruker Alpha ATR-IR spectrophotometer. MS Spectra were obtained utilizing a Waters AutoSpec-Ultima NT mass spectrometer or Waters Xero G2-XS Qtof. Elemental analyses were performed by Atlantic Microlab, Inc. UV–Vis-NIR spectra were measured with a Cary 5000 instrument and a curvature with a 1 cm path length open to ambient atmosphere.

Photocatalysis General Information. A 150 W Sciencetech SF-150C Small Collimated Beam Solar Simulator equipped with an AM 1.5 filter was used as the light source for the photocatalytic experiments. Head space analysis was performed using a VICI gas tight syringe with stopcock and a custom Agilent 7890B Gas Chromatography instrument equipped with Agilent PorapakQ 6ft, 1/8 O.D. column. Quantitation of CO and CH₄ were made using an FID detector, while H₂ was quantified using a TCD detector. All calibrations were done using standards purchased from BuyCalGas.com.

Photocatalysis Procedure. To a 17 ml vial was added BIH (0.005 g, 0.02 mmol), MeCN (6 ml, bulk or anhydrous), and catalyst (0.2 ml from 1 × 10⁻³ M in MeCN solution). The solution was bubbled vigorously with CO₂ for at least 15 minutes until the solution volume reached 1.9 ml and then 0.1 ml of degassed triethylamine was added to the mixture. The tube was sealed with a rubber septum and irradiated with a solar simulator. Head space samples were taken and the pressure was adjusted to atmospheric pressure by pressurizing the sample (300 μL taken from the headspace then compressed to 250 μL) then submerging the sealed gas tight syringe into diethyl ether. The syringe was open and gas was observed exiting the needle tip. The syringe was then sealed, removed from the diethyl ether solution and injected into the GC mentioned above.

Synthesis and Characterization of Compounds and Complexes.

Synthesis of 2,6-di(1H-imidazol-1-yl)-4-methoxypyridine (6). A Schlenk flask with stir bar was charged with sodium hydride (1.382 g, 57.58 mmol) and filled with 150 mL of DMF. With vigorous stirring and positive $N_{2(g)}$ flow, imidazole (3.9081 g, 57.405 mmol) was added portion wise to minimize effervescence. A solution of 2,6-difluoro-4-methoxypyridine¹ (**5**) (4.141 g, 28.54 mmol) and 40 mL of DMF was then added to the reaction flask via cannula transfer. The reaction flask was then joined with an oven dried and $N_{2(g)}$ purged reflux condenser under positive pressure. The solution was then heated to 70° C and stirred for 16 h. The crude reaction solution was filtered through a celite plug then the filtrate dried on a rotovap yielding the crude product as a yellow solid. The solid was purified through recrystallization in 40 mL of EtOH. The resulting solid was collected by filtration and wash with a minimal quantity of cold EtOH then cold ether. This resulted in pure product (**6**) as a white solid (5.9544 g, 86.48%). ¹H NMR: (360MHz, DMSO, RT, ppm) δ 8.76 (s, 2H, $H_{N_{CN}}$), 8.15 (t, $J=1.31$ Hz, 2H H_{im}), 7.38 (s, 2H, H_{py}), 7.15 (t, $J=1.02$ Hz, 2H, H_{im}), 4.03 (s, 3H, H_{OMe}) (see Figure S1). ¹³C NMR: (126MHz, CDCl₃, RT, ppm) δ 170.16 (s, C_{ortho}), δ 149.78 (s, C_{para}), δ 135.13 (s, $C_{N_{CN}}$), δ 131.05 (s, C_{im}), δ 116.23 (s, C_{im}), δ 96.16 (s, C_{meta}), δ 56.25 (s, C_{OMe}) (see Figure S2). ¹³C NMR: (126MHz, DMSO, RT, ppm) δ 170.76 (s, C_{ortho}), δ 149.53 (s, C_{para}), δ 136.16 (s, $C_{N_{CN}}$), δ 130.59 (s, C_{im}), δ 117.44 (s, C_{im}), δ 96.90 (s, C_{meta}), δ 57.30 (s, C_{OMe}) (see Figure S3). FT-IR (ATR, cm^{-1}): 3108 (m), 1613 (s), 1605 (s), 1503 (w), 1483 (s), 1442 (s), 1409 (w), 1307 (w), 1295 (s), 1291 (m), 1226 (s), 1219 (vs), 1205 (m), 1114 (w), 1069 (m), 1063 (s), 1014 (s), 991 (m), 977 (m), 906 (m), 863 (s), 830 (s), 755 (m), 744 (s), 657 (s), 626 (w), 600 (w), 543 (w), 471 (w) (see Figure S4). EI-HRMS (EI⁺): m/z found (expected): 242.9859 ($C_{12}H_{13}N_5O^+$, 243.1112); 241.0955 ($C_{12}H_{11}N_5O^+$, 241.0964); 230.9856 ($C_{11}H_{13}N_5O^+$, 231.1120) (see Figure S5).

Synthesis of 1,1'-(2,6-p-methoxypyridinediyl)bis[3-methyl-1H-Imidazolium] ditriflate (7). A Schlenk flask with stir bar was charged with 2,6-di(1H-imidazol-1-yl)-4-methoxypyridine (**6**) (1.5059 g, 6.2421 mmol) and filled with 35 mL of DMF. The flask was stoppered under $N_{2(g)}$ pressure and the mixture was then stirred till the solid dissolved. Methyl triflate (1.50 mL, 13.7 mmol) was added drop wise via a syringe to the reaction solution. The reaction solution was then left stirring for 16 h; a white solid precipitated out of solution. The reaction solution was then poured into a 250 mL RBF containing 125 mL of ether being stirred vigorously; after 1 h. of stirring more solid precipitate is observed. This solid was collected using a fritted filter and was rinsed with ether to yield the product (**7**) as a white solid (2.8065 g, 79.012%). ¹H NMR: (500MHz, DMSO, RT, ppm) δ 10.27 (s, 2H, $H_{N_{CN}}$), 8.75 (s, 2H, H_{im}), 8.07 (d, 2H, H_{im}), 7.84 (s, 2H, H_{py}), 4.12 (s, 3H, H_{OMe}) 4.03 (s, 6H, H_{NMe}) (see Figure S6). ¹⁹F NMR: (339MHz, DMSO, RT, ppm) δ -77.77 (s, F_{OTf}) (see Figure S7). ¹³C NMR: (126MHz, DMSO, RT, ppm) δ 171.07 (s, C_{para}), δ 146.54 (s, C_{ortho}), δ 136.15 (s, $C_{N_{CN}}$), δ 124.87 (s, C_{im}), δ 120.59 (q, $J=323.10$ Hz, C_{OTf}), δ 119.07 (s, C_{im}), δ 100.49 (s, C_{meta}), δ 57.69 (s, C_{OMe}), δ 36.52 (s, C_{NMe}) (see Figure S8). FT-IR (ATR, cm^{-1}): 3155 (w), 3098 (m), 3066 (w), 1623 (s), 1585 (m), 1544 (s), 1493 (m), 1460 (m),

1356 (w), 1246 (vs), 1228 (vs), 1224 (vs), 1156 (s), 1030 (vs), 1018 (s), 973 (m), 971 (m), 865 (m), 761 (m), 754 (m), 636 (vs), 620 (s), 575 (m), 518 (s), 509 (w), 414 (w) (see Figure S9). ESI-MS (ESI⁺): m/z found (expected): 420.0950 [(CNC-OMe)OTf]⁺ = C₁₅H₁₇F₃N₅O₄S⁺, 420.0953), 270.1359 [(CNC-OMe)-H]⁺ = C₁₄H₁₆N₅O⁺, 270.1355) (see Figure S10).

Synthesis of [Ru(CNC-OMe)(ACN)₂Cl]OTf (2). A Schlenk flask was charged with 1,1'-(2,6-p-methoxyppyridinediyl)bis[3-methyl-1H-Imidazolium] ditriflate (**7**) (0.3293 g, 0.5787 mmol), cesium carbonate (0.4656 g, 1.429 mmol), and [RuCymCl₂]₂ (0.1540 g, 0.2515 mmol) and filled with acetonitrile (30 mL) resulting in a light orange mixture. The reaction solution was heated to 70°C for 2 h; during which there was considerable quantity of precipitate that formed. The reaction was cooled and allowed to stir for 16h. During which the precipitate dissolved and the reaction solution darkened. The reaction solution was then poured through a silica plug and the filtrate was dried via a rotovap. The product (**2**) is obtained as a yellow solid residue (0.2651 g, 82.75%). ¹H NMR: (360MHz, CD₃CN, RT, ppm) δ 7.91 (d, J=2.28 Hz, 2H, H_{im}), 7.29 (d, J=2.17 Hz, 2H, H_{im}), 7.11 (s, 2H, H_{py}), 4.11 (s, 6H, H_{NMe}), 4.01 (s, 3H, H_{OMe}), 2.53 (s, 3H, H_{ACN}), 1.86 (s, 3H, H_{ACN}) (see Figure S11). ¹H NMR: (500MHz, DMSO, RT, ppm) δ 8.43 (d, J=1.86 Hz, 2H, H_{im}), 7.63 (d, J=1.99 Hz, 2H, H_{im}), 7.59 (s, 2H, H_{py}), 4.10 (s, 6H, H_{NMe}), 4.05 (s, 3H, H_{OMe}), 2.71 (s, 3H, H_{ACN}), 2.10 (s, 3H, H_{ACN}) (see Figure S12). ¹⁹F NMR: (339MHz, CD₃CN, RT, ppm) δ -79.38 (s, F_{OTf}) (see Figure S13). ¹⁹F NMR: (360MHz, DMSO, RT, ppm) δ -77.76 (s, F_{OTf}). ¹³C NMR: (126MHz, DMSO, RT, ppm) δ 197.25 (s, C_{N-CN}), δ 169.51 (s, C_{para}), δ 156.24 (s, C_{ortho}), δ 127.20 (s, C_{ACN-CN}), δ 124.64 (s, C_{im}), δ 123.84 (s, C_{ACN-CN}), δ 121.16 (q, J=323.10 Hz, C_{OTf}), δ 118.00 (s, C_{im}), δ 93.41 (s, C_{meta}), δ 57.78 (s, C_{OMe}), δ 37.37 (s, C_{NMe}), δ 4.03 (s, C_{ACN-Me}), δ 3.89 (s, C_{ACN-Me}) (see Figure S14). FT-IR (ATR, cm⁻¹): 3114 (w), 3083 (w), 2984 (vw), 2929 (vw), 2287 (vw), 2264 (w), 1630 (s), 1580 (m), 1555 (m), 1482 (s), 1454 (m), 1424 (w), 1404 (m), 1349 (m), 1263 (vs), 1238 (vs), 1222 (vs), 1137 (s), 1083 (vs), 970 (m), 943 (w), 874 (w), 841 (m), 790 (w), 746 (m), 699 (s), 636 (vs), 587 (m), 571 (m), 516 (s), 430 (w) (see Figure S15). ESI-HRMS (ESI⁺): m/z found (expected): 488.0547 ([Ru(CNC-OMe)(ACN)₂Cl]⁺ = C₁₈H₂₁ClN₇ORu⁺, 488.0572), 447.0276 ([Ru(CNC-OMe)(ACN)Cl]⁺ = C₁₆H₁₈ClN₆ORu⁺, 447.0306), 406.0018 ([Ru(CNC-OMe)Cl]⁺ = C₁₄H₁₅ClN₅ORu⁺, 406.0041), 226.5429 ([Ru(CNC-OMe)(ACN)₂]²⁺ = C₁₈H₂₁N₇ORu²⁺, 226.5442), 206.0283 ([Ru(CNC-OMe)(ACN)]²⁺ = C₁₆H₁₈N₆ORu²⁺, 206.0309) (see Figure S17). Anal. Calcd. for C₁₉H₂₁O₄N₇SF₃ClRu: C, 35.82; H, 3.32; N, 15.39. Found: C, 35.67; H, 3.23; N, 15.18.

Synthesis of [Ru(CNC-OMe)(ACN)₃](OTf)₂ (3). A Schlenk flask was loaded with [Ru(CNC-OMe)(ACN)₂Cl]OTf (**2**) (0.2270 g, 0.3564 mmol) and silver triflate (0.1177 g, 0.4581 mmol) and filled with acetonitrile (20 mL). The reaction solution was then heated to 70°C; after which a white precipitate was noted. Heating for 2 h. led to a pale yellow reaction solution. The reaction was left heating overnight to obtain a pale yellow solution with a white solid. The reaction

solution was filtered through a silica plug. The pale yellow filtrate was dried down yielding the product (**3**) as an off white solid (0.2821 g, 93.9%). ¹H NMR: (360MHz, DMSO, RT, ppm) δ 8.54 (d, J=2.13 Hz, 2H, H_{im}), 7.75 (d, J= 2.13 Hz, 2H, H_{im}), 7.74 (s, 2H, H_{py}), 4.11 (s, 6H, H_{NMe}), 4.09 (s, 3H, H_{OMe}), 2.75 (s, 3H, H_{ACN}), 2.14 (s, 3H, H_{ACN}) (see Figure S18). ¹⁹F NMR: (339MHz, DMSO, RT, ppm) δ -77.76 (s, F_{OTf}) (see Figure S19). ¹³C NMR: (126MHz, DMSO, RT, ppm) δ 190.47 (s, C_{NCN}), δ 170.46 (s, C_{para}), δ 155.11 (s, C_{ortho}), δ 128.11 (s, C_{ACN-CN}), δ 125.06 (s, C_{ACN-CN}), δ 125.02 (s, C_{im}), δ 120.67 (q, J=321.41 Hz, C_{OTf}), δ 118.30 (s, C_{im}), δ 94.28 (s, C_{meta}), δ 57.67 (s, C_{OMe}), δ 37.18 (s, C_{NMe}), δ 3.61 (s, C_{ACN-Me}), δ 3.24 (s, C_{ACN-Me}) (see Figure S20). FT-IR (ATR, cm⁻¹): 3123 (w), 3096 (w), 2917 (w), 2266 (w), 1642 (m), 1581 (w), 1554 (w), 1491 (m), 1475 (m), 1413 (w), 1344 (w), 1244 (vs), 1242 (vs), 1222(vs), 1193 (s), 1163 (s), 1161 (s), 1030 (vs), 1001 (w), 877 (w), 828 (w), 765 (w), 698 (m), 636 (vs), 571 (m), 516 (s), 436 (w) (see Figure S21). ESI-HRMS (ESI⁺): m/z found (expected): 643.0637 ([Ru(CNC-OMe)(ACN)₃]OTf⁺ = C₂₁H₂₄F₃N₈O₄RuS⁺, 643.0657), 602.0383 ([Ru(CNC-OMe)(ACN)₂]OTf⁺ = C₁₉H₂₁F₃N₇O₄RuS⁺, 602.0371), 561.0102 ([Ru(CNC-OMe)(ACN)]OTf⁺ = C₁₇H₁₈F₃N₆O₄RuS⁺, 561.0106), 247.0555 ([Ru(CNC-OMe)(ACN)₃]²⁺ = C₂₀H₂₄N₈ORu²⁺, 247.0575), 226.5429 ([Ru(CNC-OMe)(ACN)₂]²⁺ = C₁₈H₂₁N₇ORu²⁺, 226.5442), 206.0312 ([Ru(CNC-OMe)(ACN)]²⁺ = C₁₆H₁₈N₆ORu²⁺, 206.0309) (see Figure S22-24). Complex **3** is less stable than complex **2** and a suitable analysis (performed off site and shipped) could not be obtained.

Synthesis of [Ru(CNC-H)(ACN)₂Cl]OTf (4**).** The synthesis of **4** followed procedure used to make **2**, starting with 1,1'-(2,6-pyridinediyl)bis[3-methyl-1H-Imidazolium] ditriflate (0.3000 g, 0.5561 mmol), cesium carbonate (0.4680 g, 1.436 mmol), and [Ru(Cym)Cl₂]₂ (0.1534 g, 0.2505 mmol) to yield an orange solid (**4**) (0.2799 g, 0.4611 mmol, 92.04%). ¹H NMR: (500MHz, DMSO, RT, ppm) δ 8.44 (s, 2H, H_{im}), 8.03 (t, J= 8.11 Hz, 1H, H_{p-py}), 7.84 (d, 8.11 Hz, 2H, H_{o-py}), 7.66 (s, 2H, H_{im}), 4.12 (s, 6H, H_{NMe}), 2.74 (s, 3H, H_{ACN}), 2.09 (s, 3H, H_{ACN}) (see Figure S25). ¹⁹F NMR: (339MHz, CD₃CN, RT, ppm) δ -77.75 (s, F_{OTf}) (see Figure S26). ¹³C NMR: (126MHz, DMSO, RT, ppm) δ 195.75 (s, C_{NCN}), δ 155.60 (s, C_{ortho}), δ 138.96 (s, C_{para}), δ 127.49 (s, C_{ACN-CN}), δ 124.23 (s, C_{im}), δ 123.17 (s, C_{ACN-CN}), δ 120.60 (q, J=322.60 Hz, C_{OTf}), δ 117.51 (s, C_{im}), δ 105.09 (s, C_{meta}), δ 36.78 (s, C_{NMe}), δ 3.47 (s, C_{ACN-Me}), δ 3.30 (s, C_{ACN-Me}) (see Figure S27). FT-IR (ATR, cm⁻¹): 3098 (w), 2269 (w), 1613 (w), 1580 (w), 1556 (w), 1486 (m), 1398 (w), 1346 (w), 1256 (vs), 1228 (vs), 1149 (vs), 1029 (vs), 940 (m), 784 (m), 759 (m), 739 (m), 719 (m), 699 (w), 671 (m), 628 (vs), 573 (s), 513 (s), 426 (m) (see Figure S28). ESI-MS (ESI⁺): m/z found (expected): 458.0446 ([Ru(CNC-H)(ACN)₂Cl]⁺ = C₁₇H₁₉ClN₇Ru⁺, 458.0435) (see Figure S29).

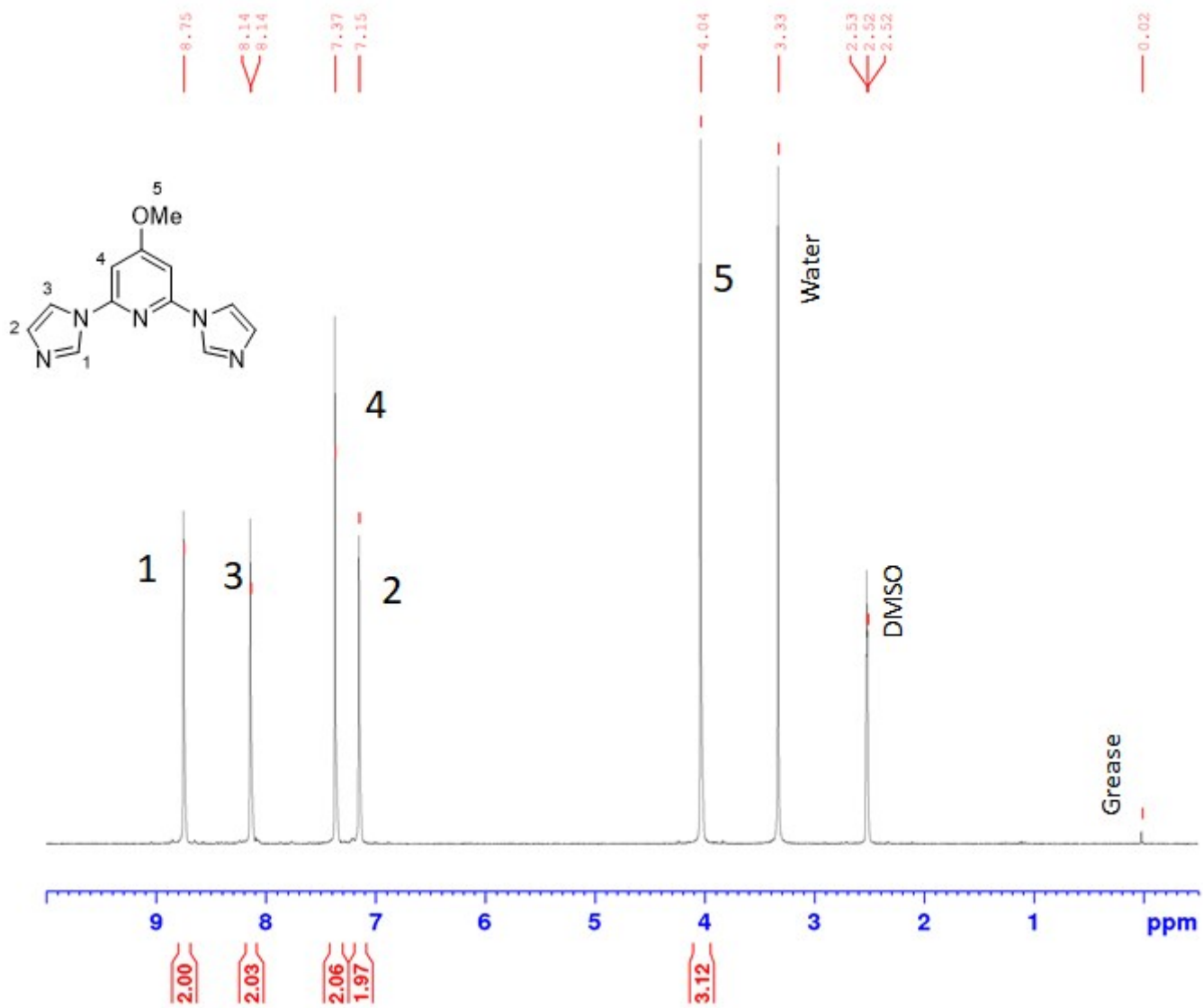


Figure S1: ¹H-NMR (360 MHz) of 2,6-di(1H-imidazol-1-yl)-4-methoxypyridine (**6**) in DMSO.

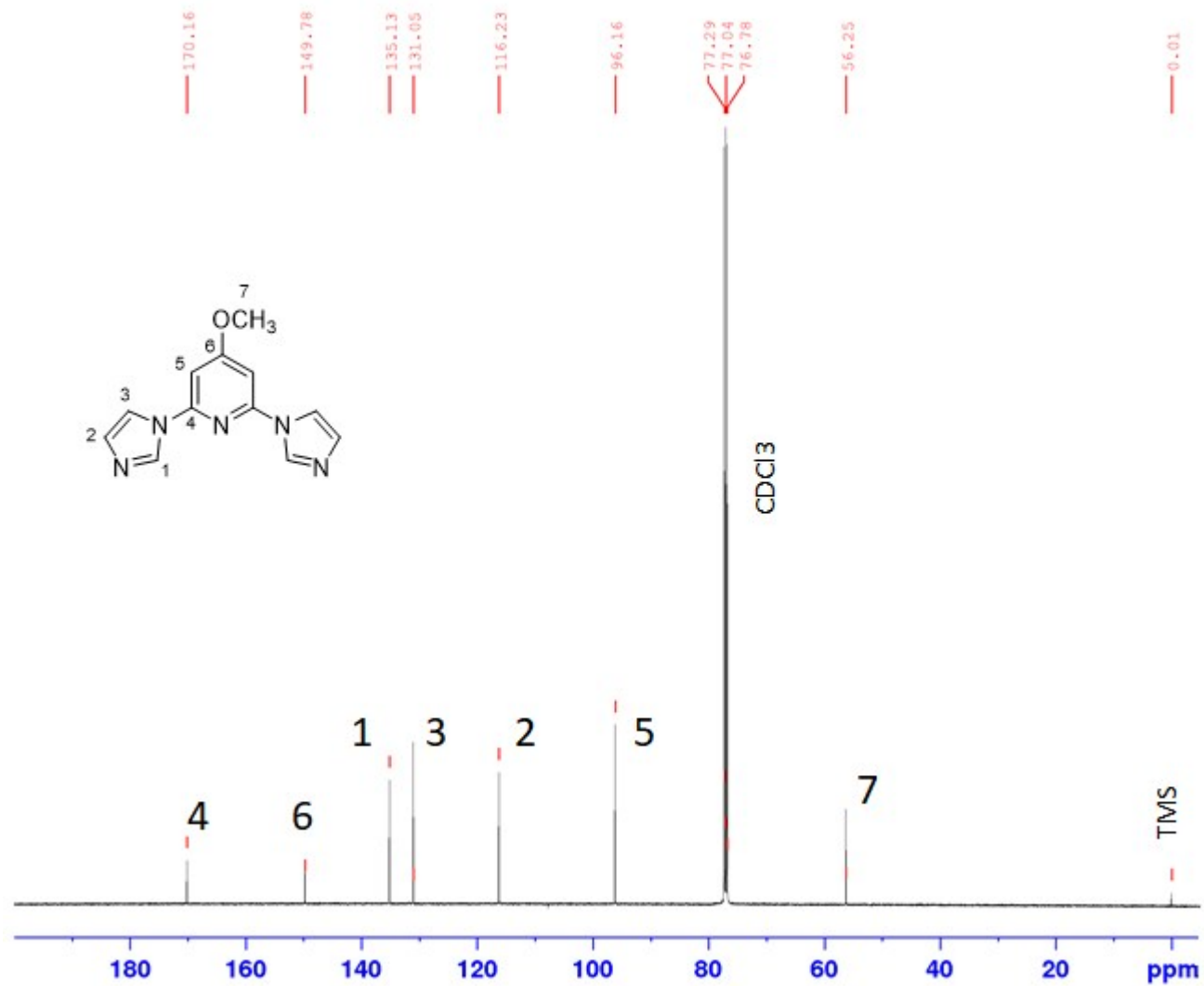


Figure S2: ¹³C-NMR (126 MHz) of 2,6-di(1H-imidazol-1-yl)-4-methoxypyridine (6) in CDCl₃.

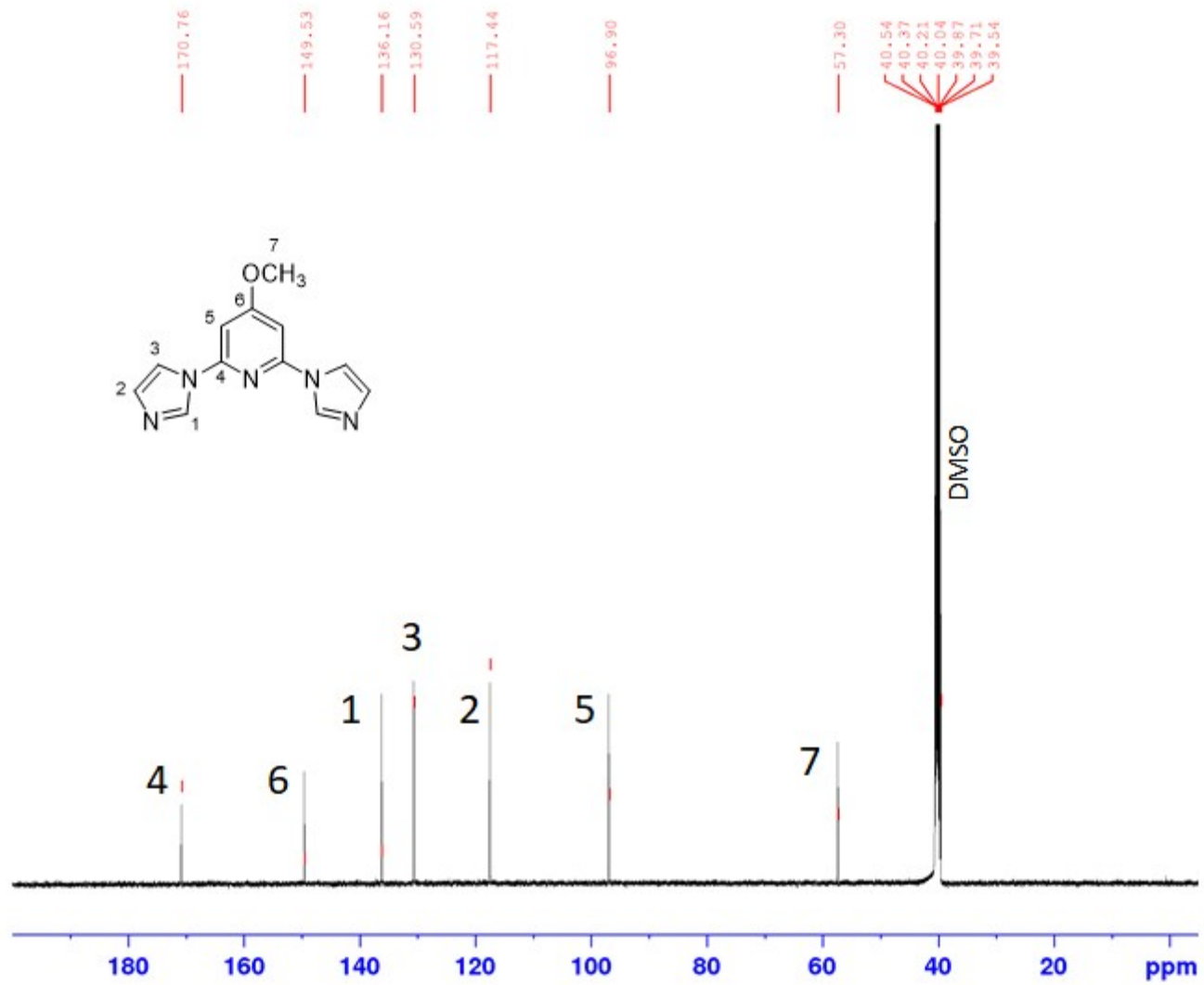


Figure S3: ¹³C-NMR (126 MHz) of 2,6-di(1H-imidazol-1-yl)-4-methoxypyridine (6) in DMSO.

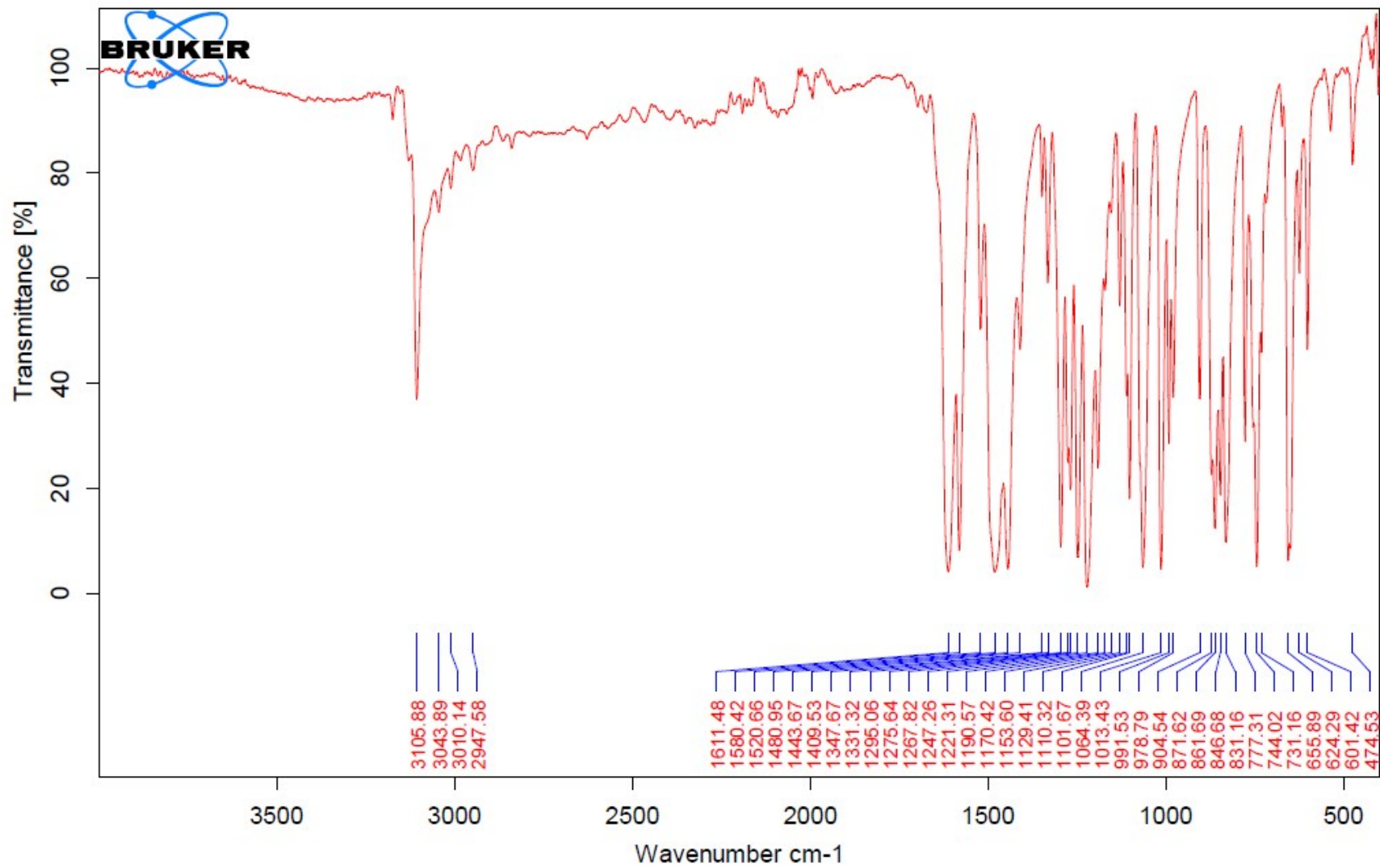


Figure S4: FT-IR (ATR) of 2,6-di(1H-imidazol-1-yl)-4-methoxypyridine (**6**), neat.

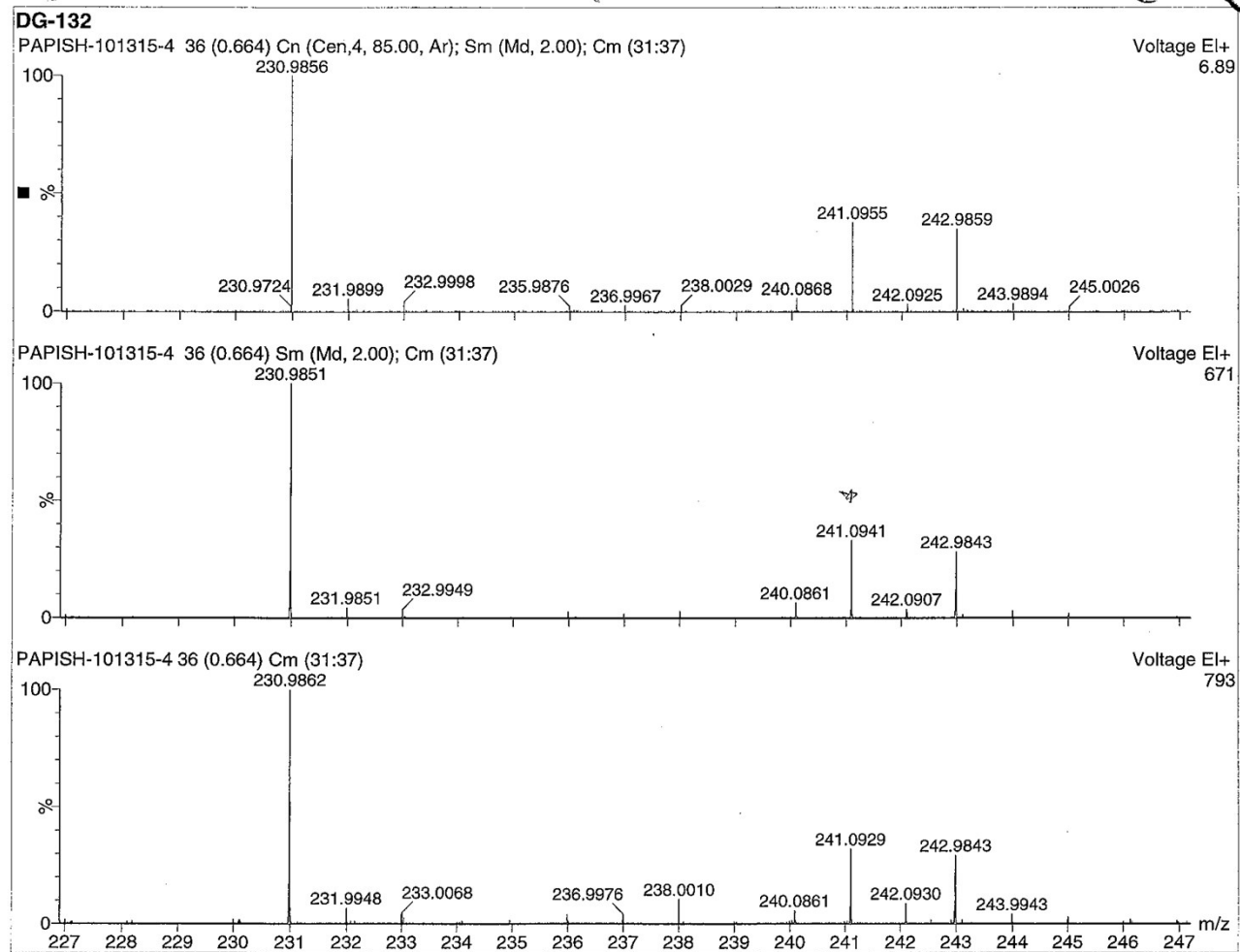


Figure S5: EI-MS (EI⁺) of 2,6-di(1H-imidazol-1-yl)-4-methoxypyridine (**6**).

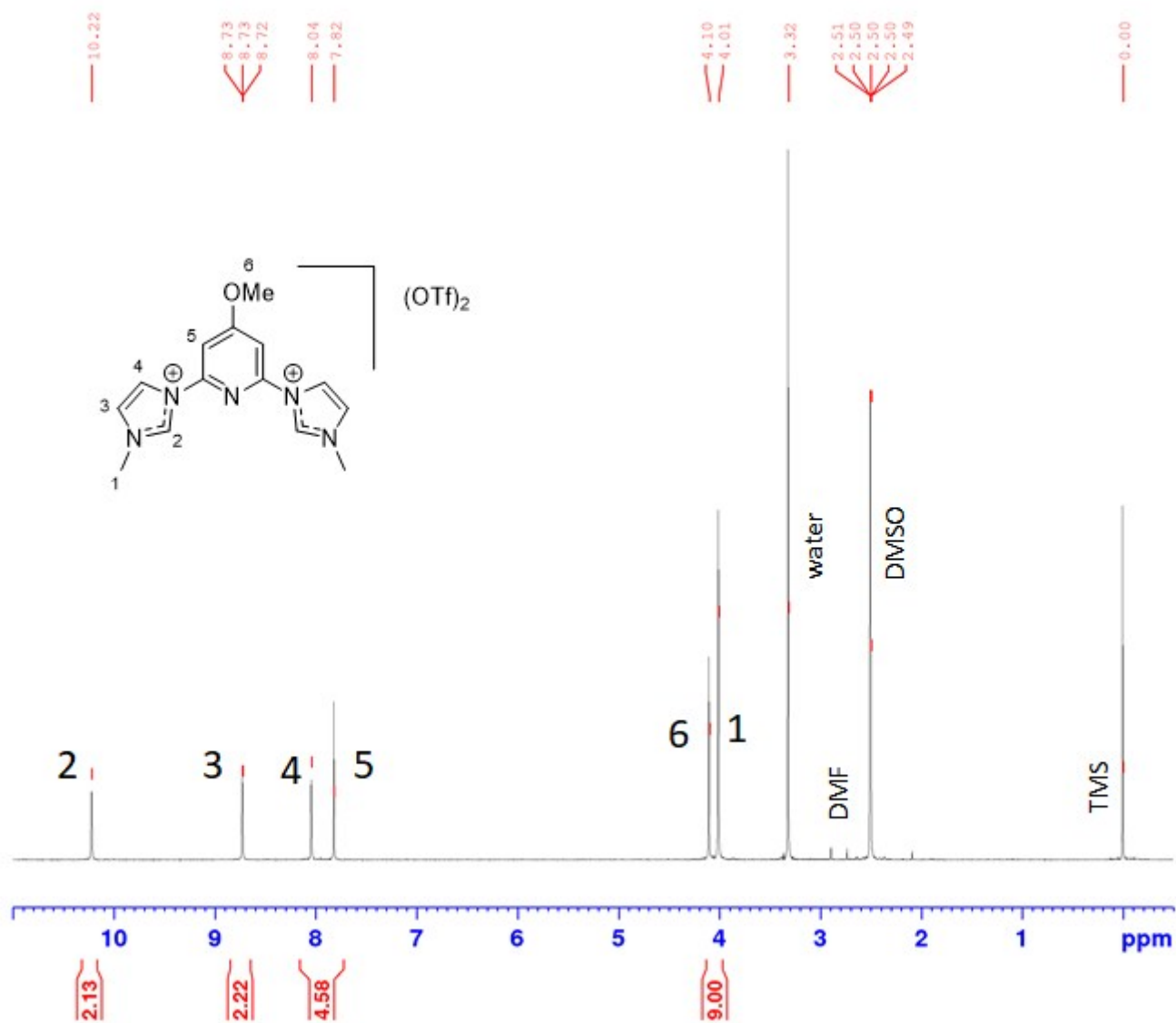


Figure S6: ¹H-NMR (500 MHz) of 1,1'-(2,6-p-methoxypyridinediyl)bis[3-methyl-1H-imidazolium] ditriflate (7) in DMSO.

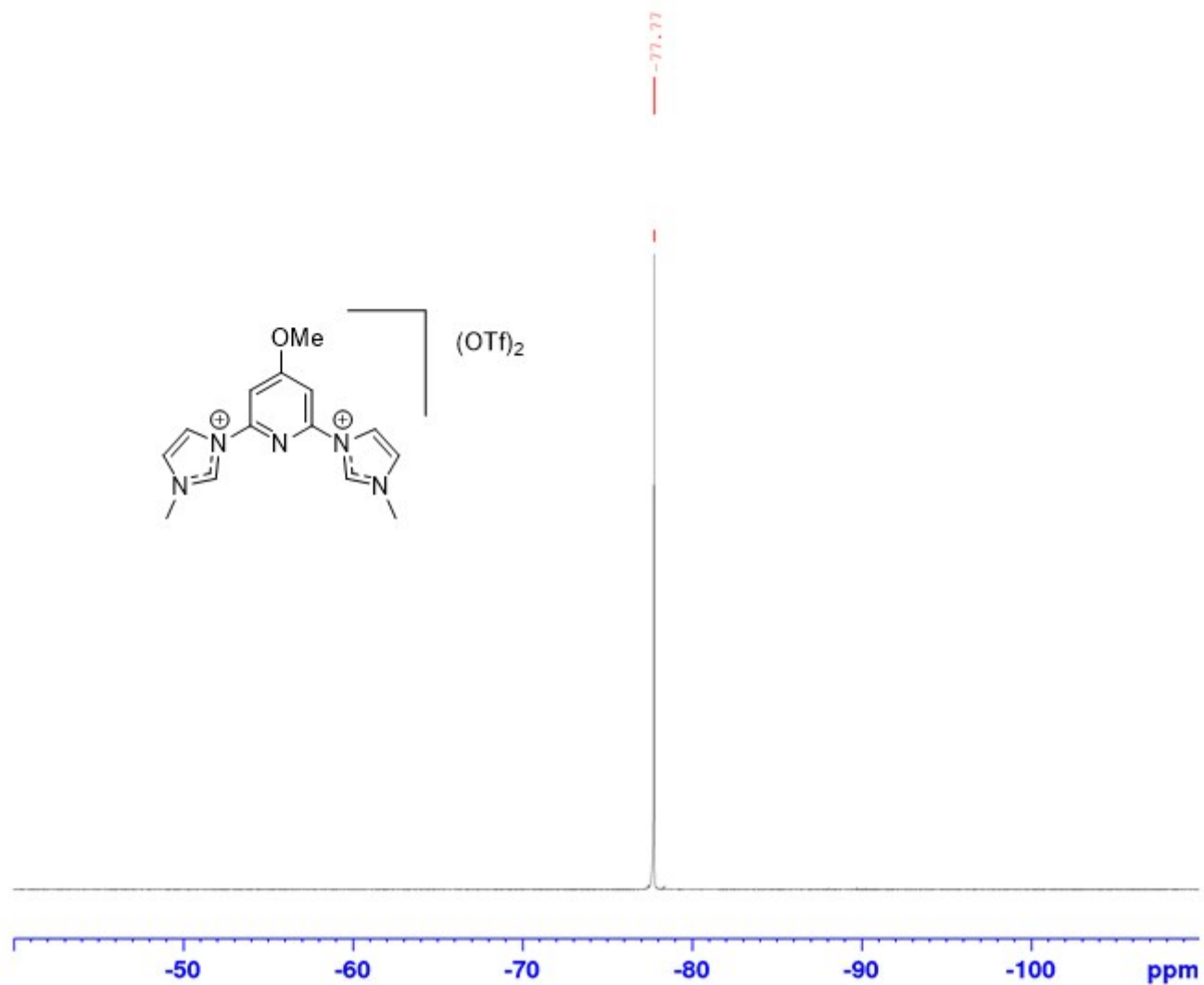


Figure S7: ^{19}F -NMR (339 MHz) of 1,1'-(2,6-p-methoxypyridinediyl)bis[3-methyl-1H-Imidazolium] ditriflate (**7**) in DMSO.

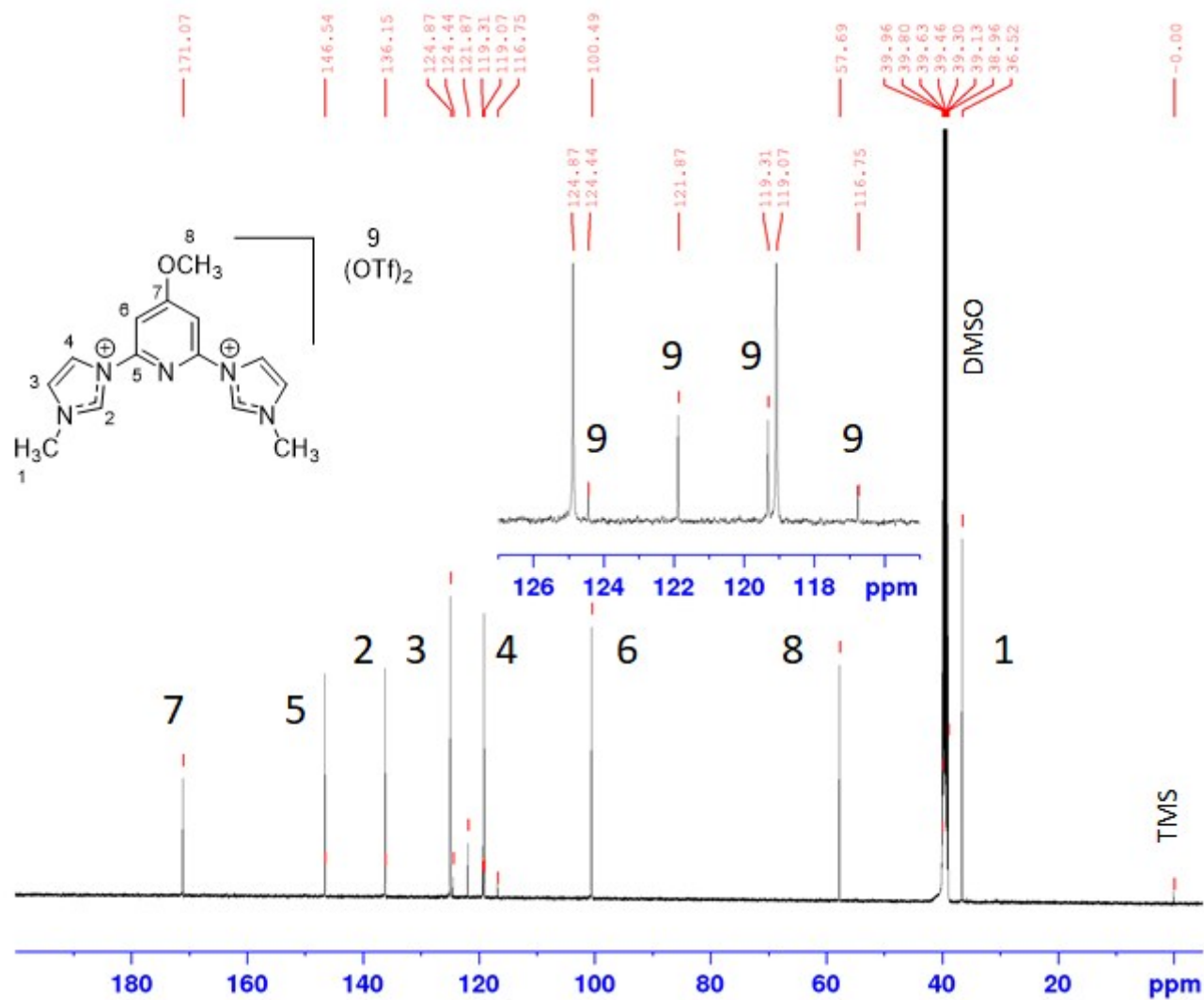


Figure S8: ¹³C-NMR (126 MHz) of 1,1'-(2,6-p-methoxypyridinediyl)bis[3-methyl-1H-imidazolium] ditriflate (7) in DMSO.

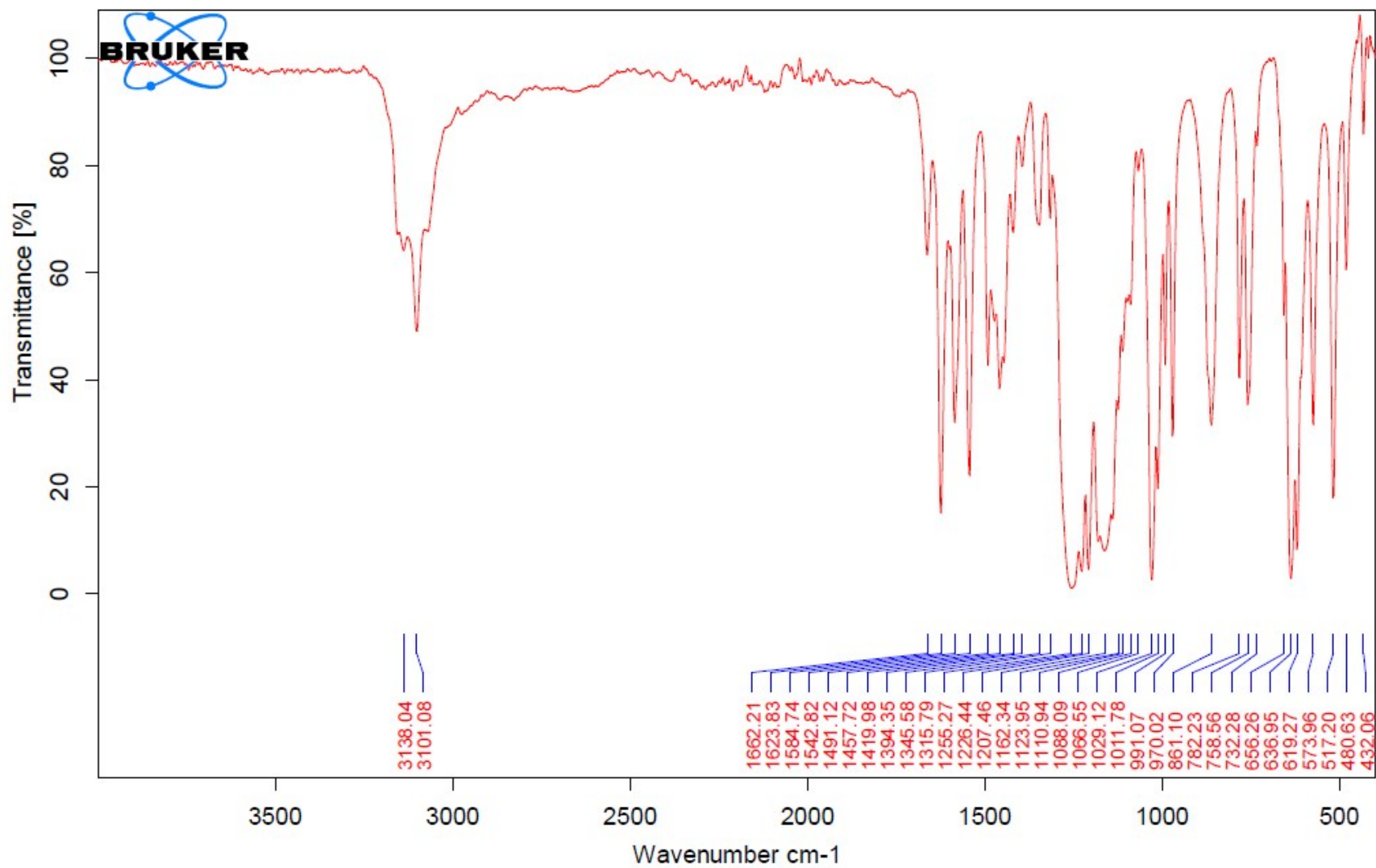


Figure S9: FT-IR (ATR) of 1,1'-(2,6-p-methoxypyridinediyl)bis[3-methyl-1H-imidazolium] ditriflate (**7**), neat.

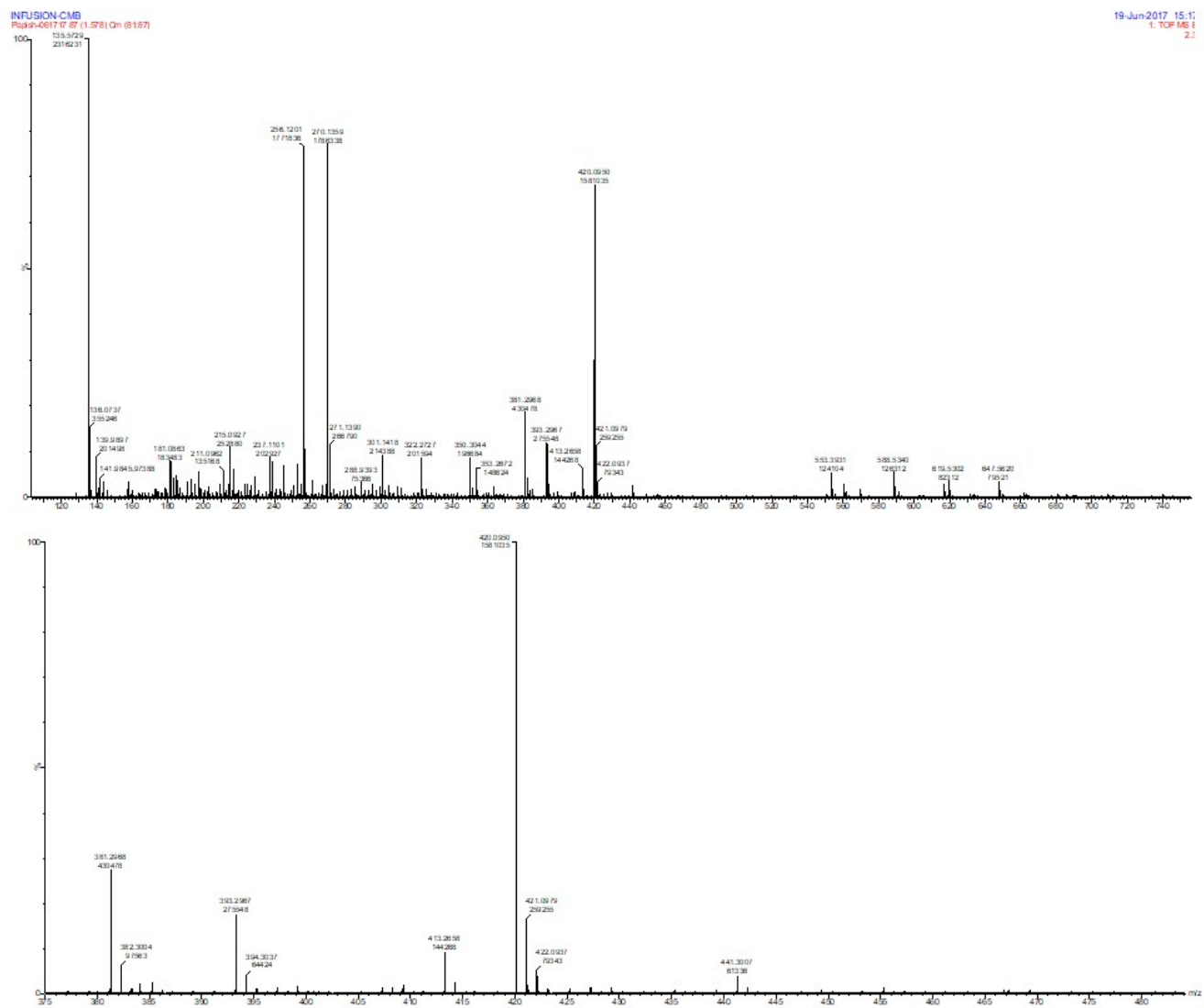


Figure S10: EI-MS (EI⁺) of 1,1'-(2,6-p-methoxypyridinediyl)bis[3-methyl-1H-Imidazolium] ditriflate (7).

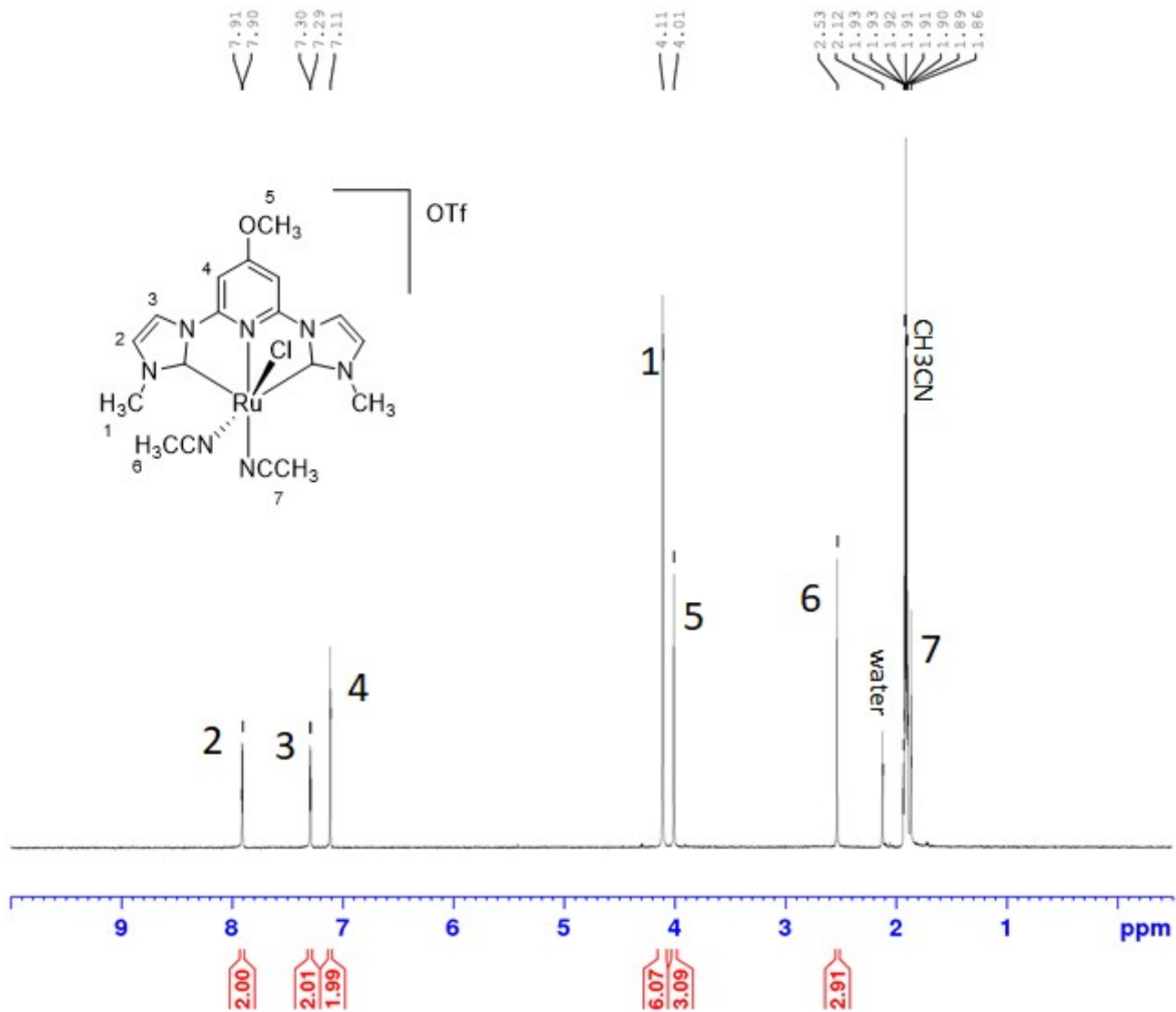


Figure S11: $^1\text{H-NMR}$ (360 MHz) of $[\text{Ru}(\text{CNC-OMe})(\text{ACN})_2\text{Cl}]\text{OTf}$ (**2**) in CD_3CN .

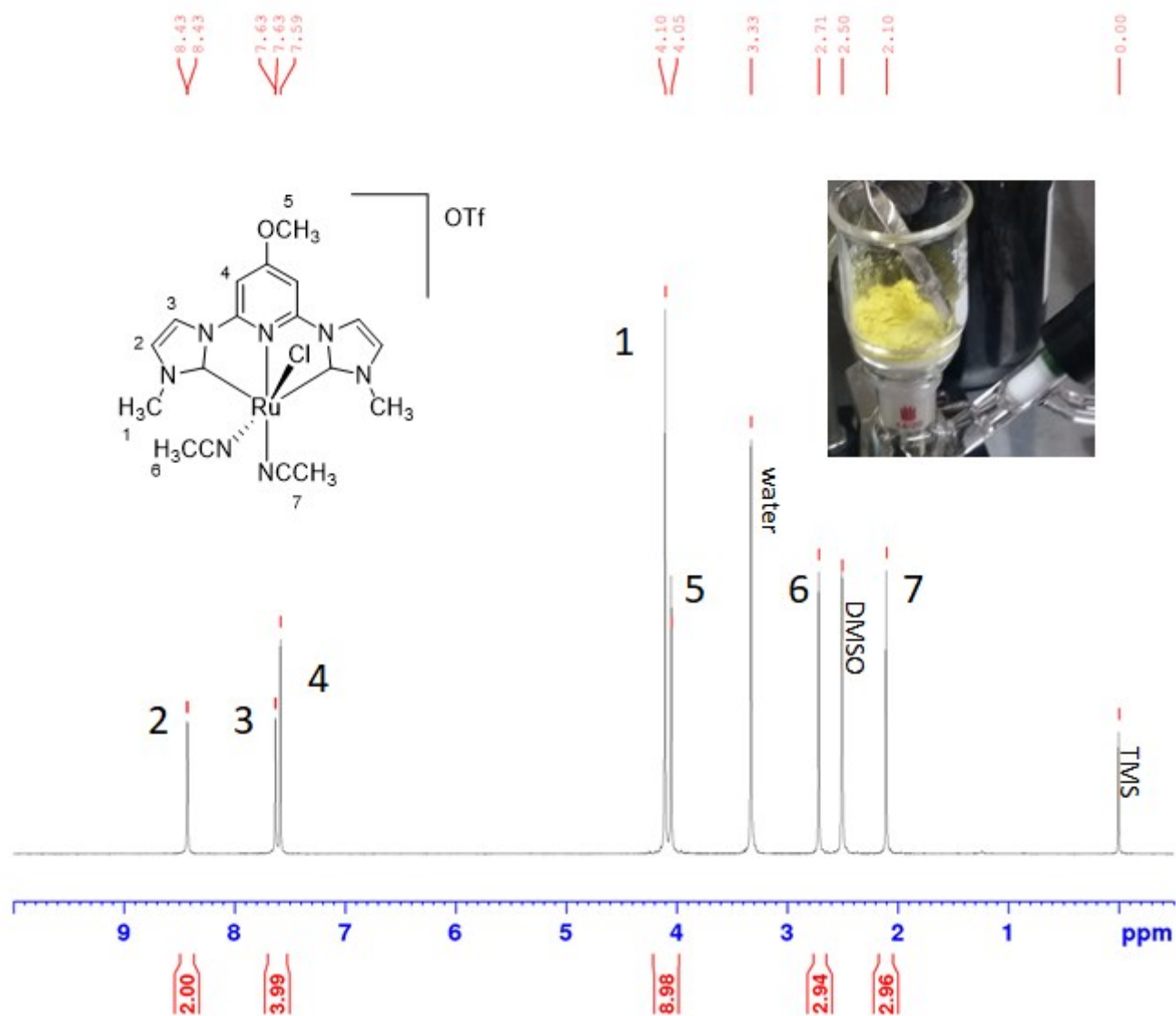


Figure S12: ¹H-NMR (500 MHz) of [Ru(CNC-OMe)(ACN)₂Cl]OTf (**2**) in DMSO.

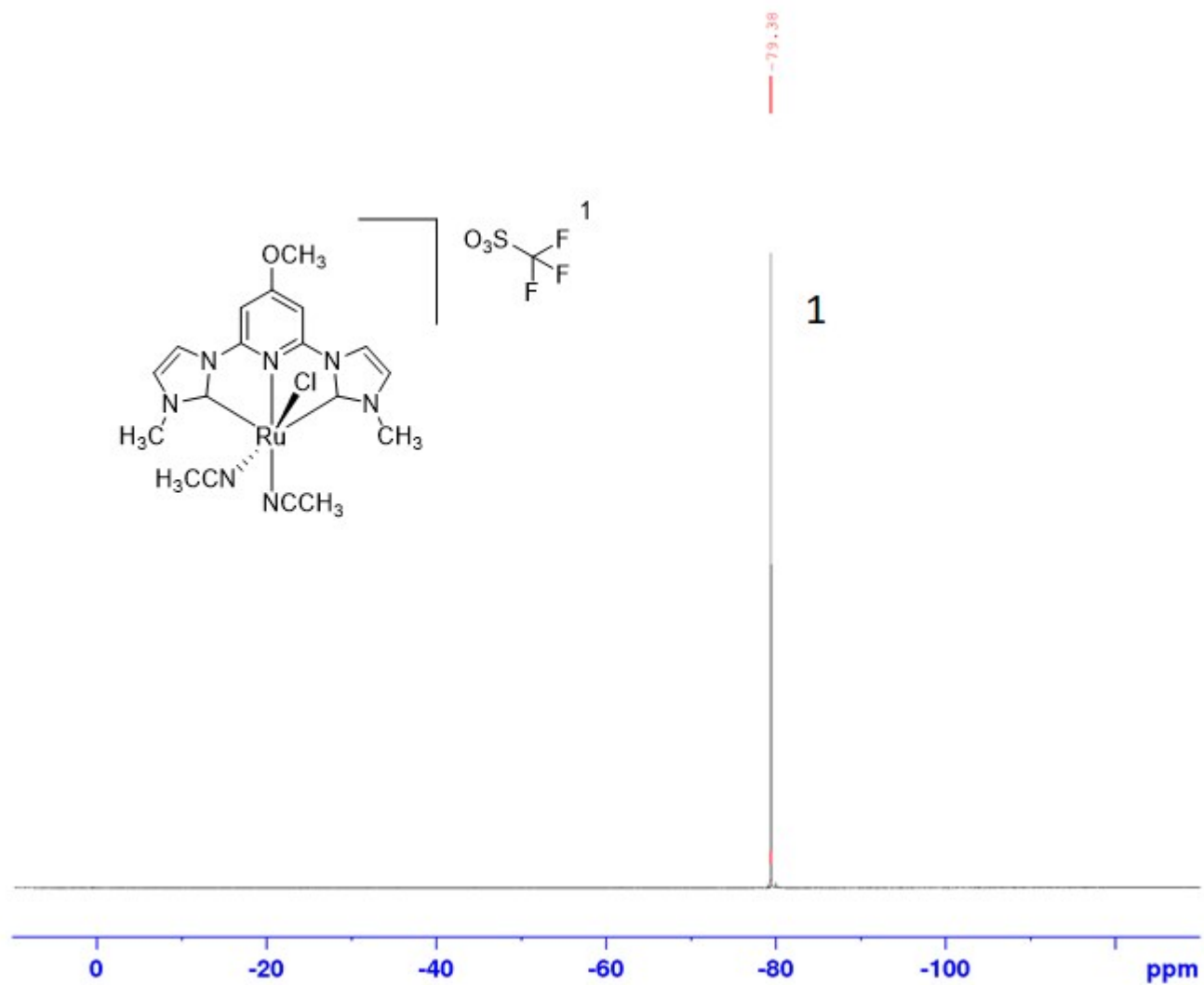


Figure S13: ^{19}F -NMR (339 MHz) of $[\text{Ru}(\text{CNC-OMe})(\text{ACN})_2\text{Cl}]\text{OTf}$ (**2**) in CD_3CN .

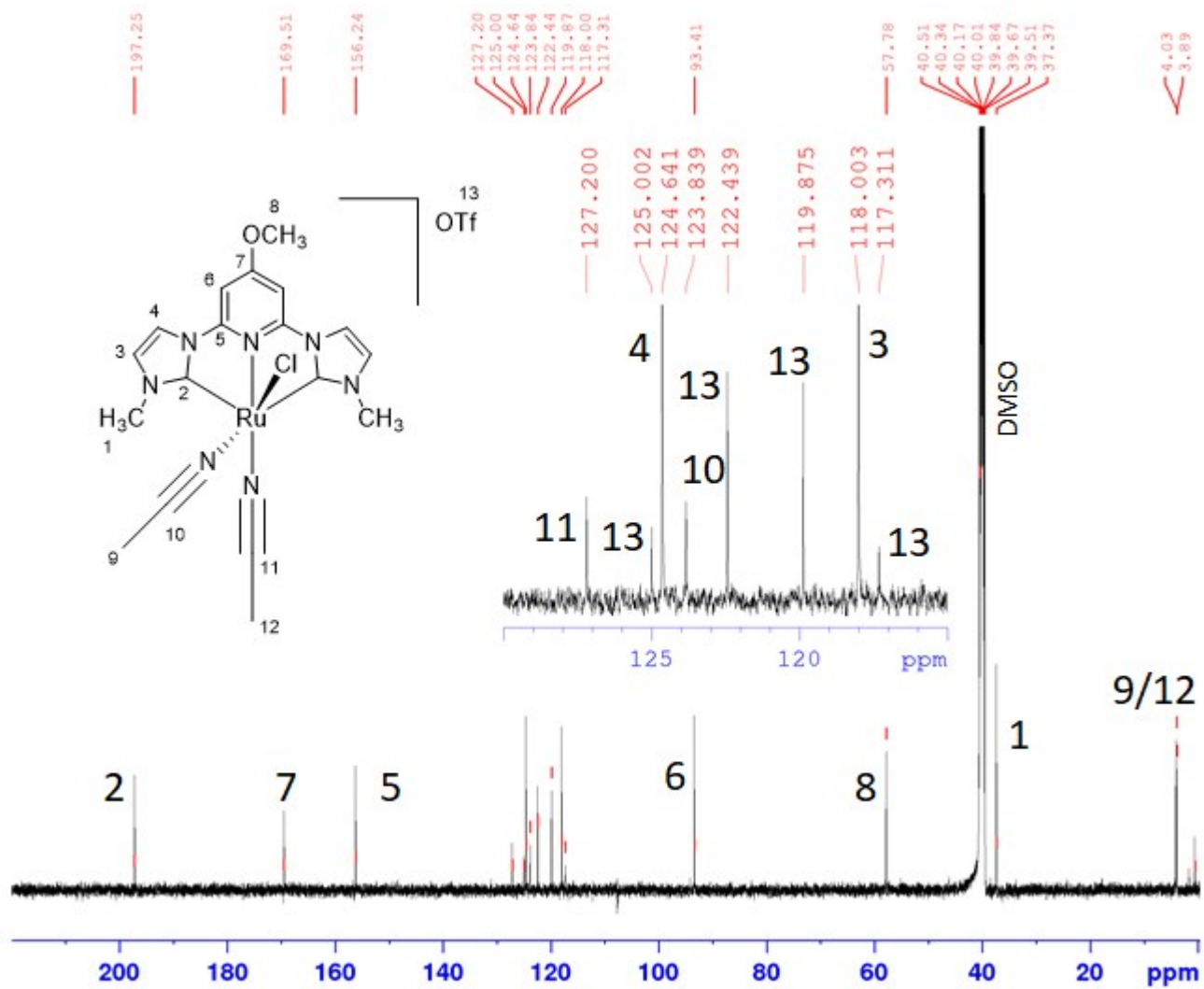


Figure S14: ^{13}C -NMR (126 MHz) of $[\text{Ru}(\text{CNC-OMe})(\text{ACN})_2\text{Cl}]\text{OTf}$ (**2**) in DMSO.

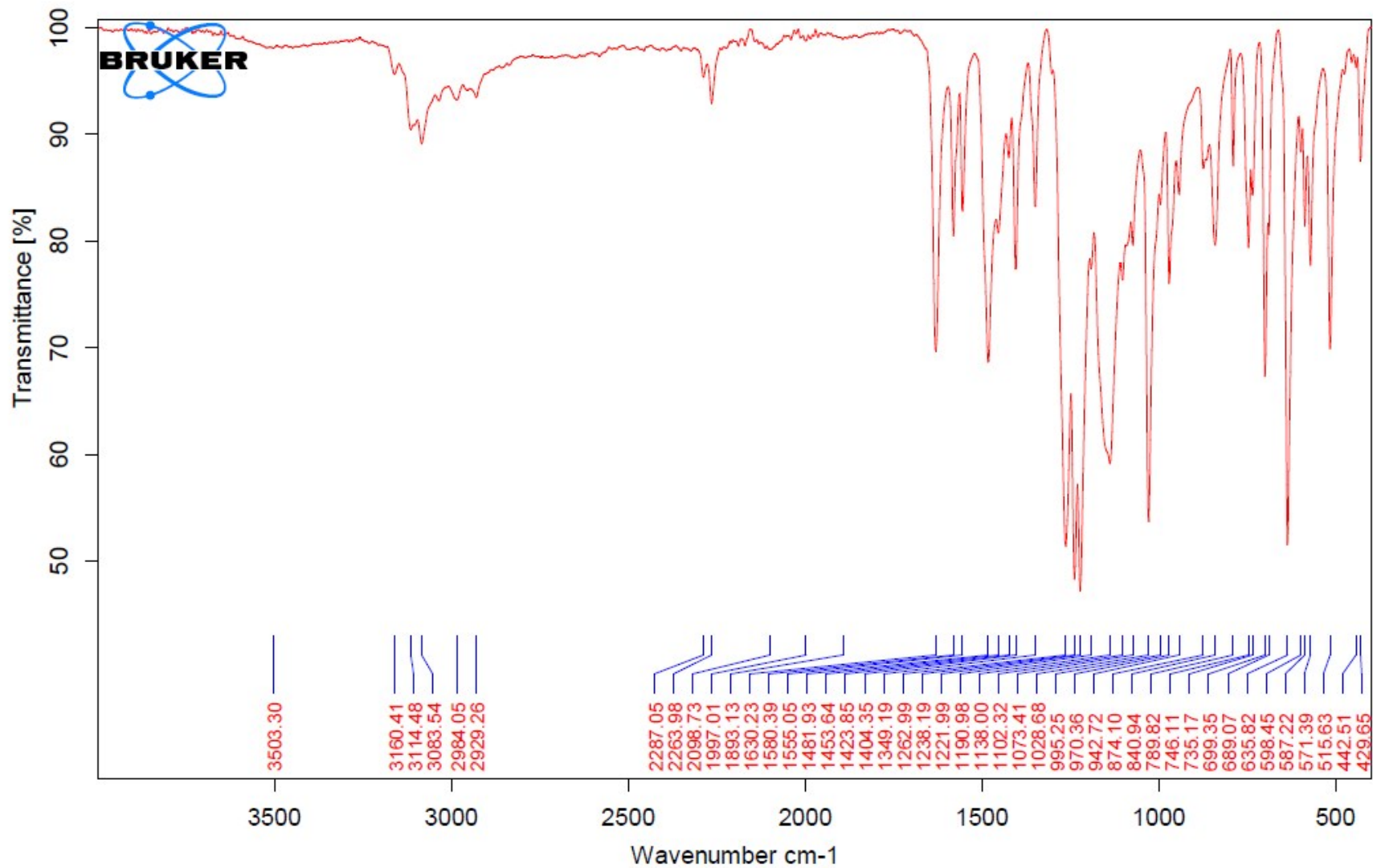


Figure S15: FT-IR (ATR) of [Ru(CNC-OMe)(ACN)₂Cl]OTf (**2**), neat.

CMB174 ACN
PAPISH-030017-3 79 (1.434 Cm (79.88)

08-Mar-2017 14:42:45
1.7CF MS ES-
6.91e5

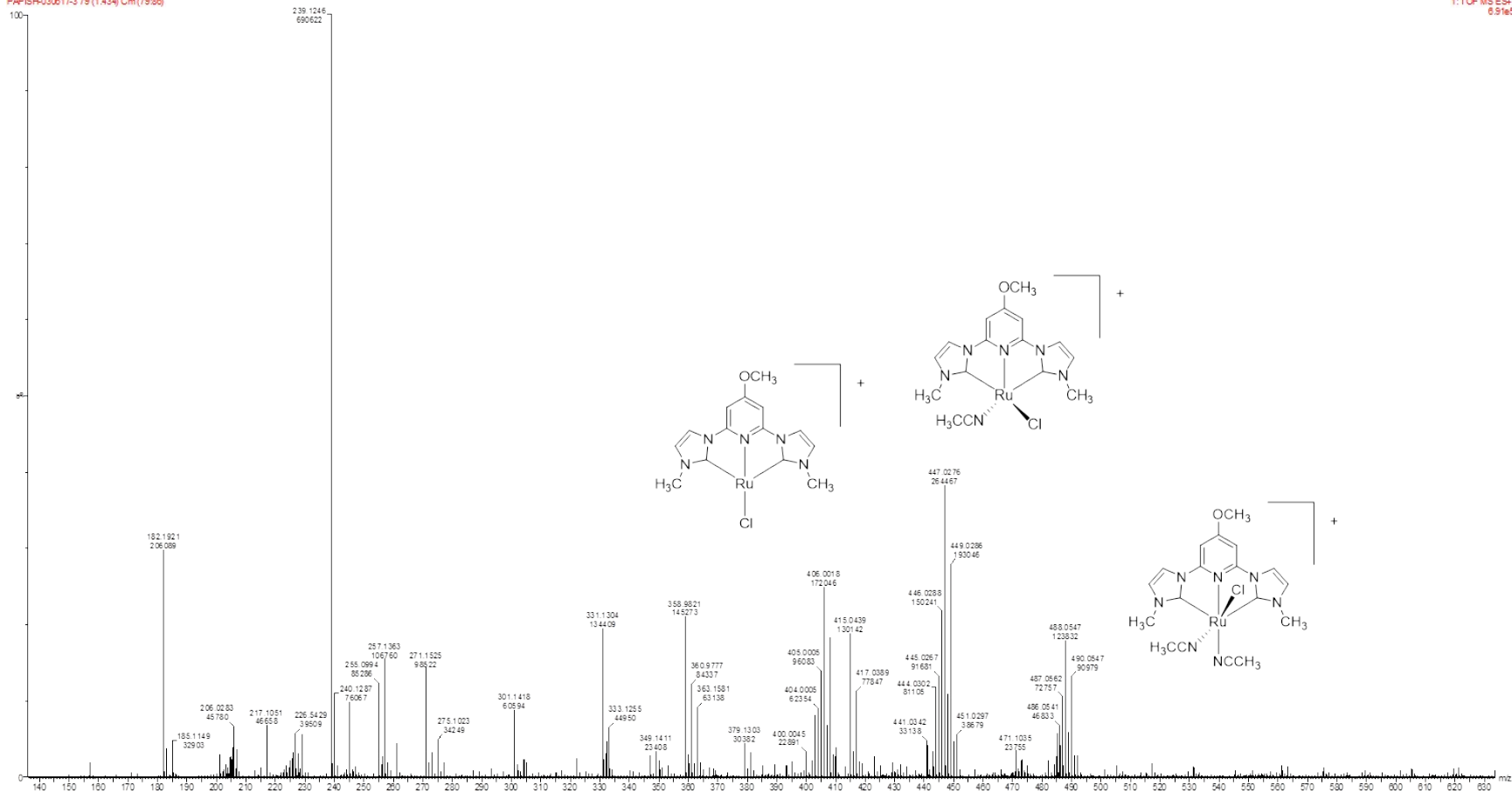
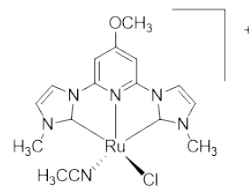


Figure S16: ESI-MS (ESI⁺) of [Ru(CNC-OMe)(ACN)₂Cl]OTf (**2**).



06-Mar-2017 14:42:46
1: TOF MS ES+
2.64e5

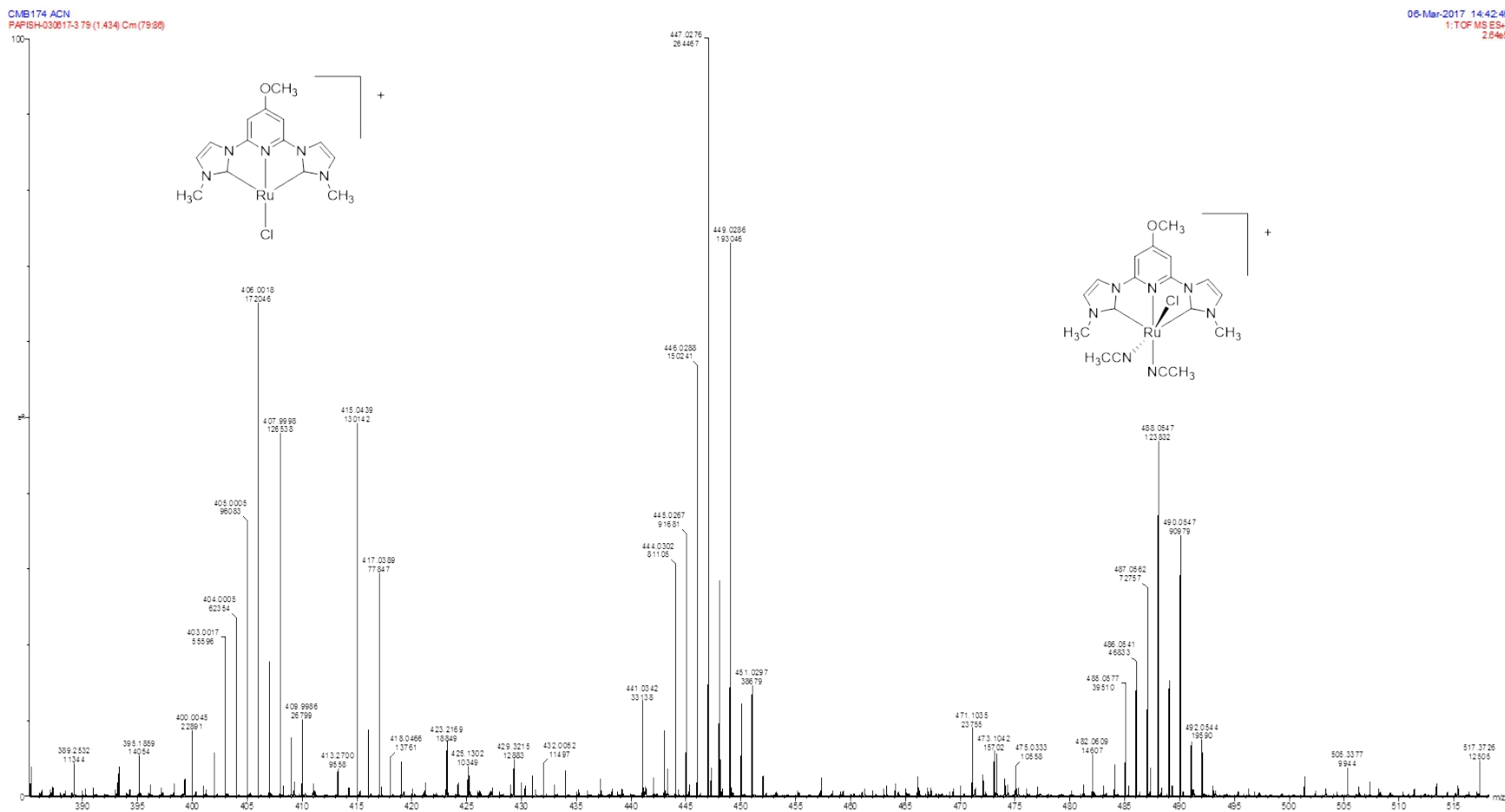


Figure S17: ESI-MS (ESI⁺) of [Ru(CNC-OMe)(ACN)₂Cl]OTf (2).

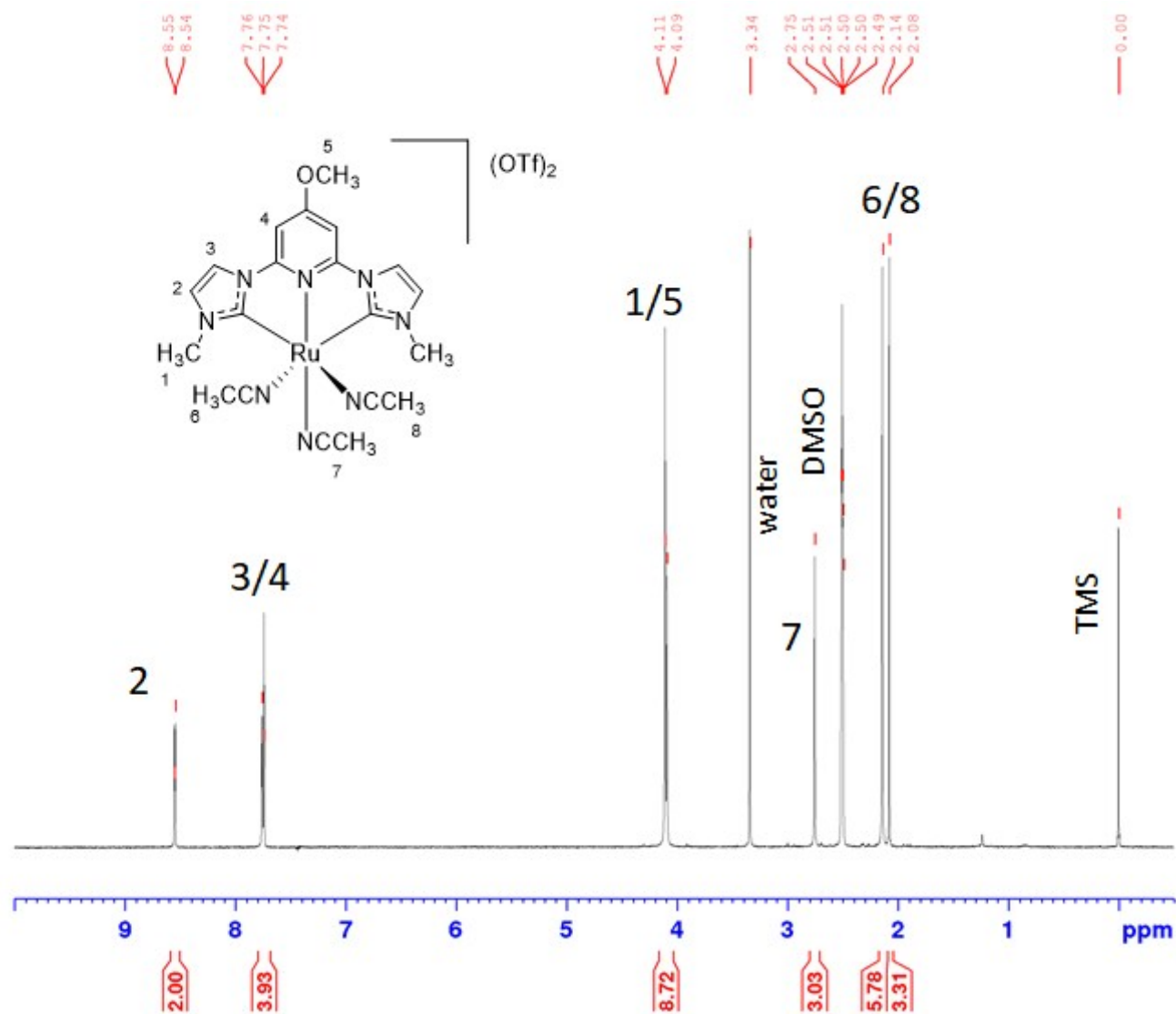


Figure S18: $^1\text{H-NMR}$ (360 MHz) of $[\text{Ru}(\text{CNC-OMe})(\text{ACN})_3](\text{OTf})_2$ (**3**) in DMSO.

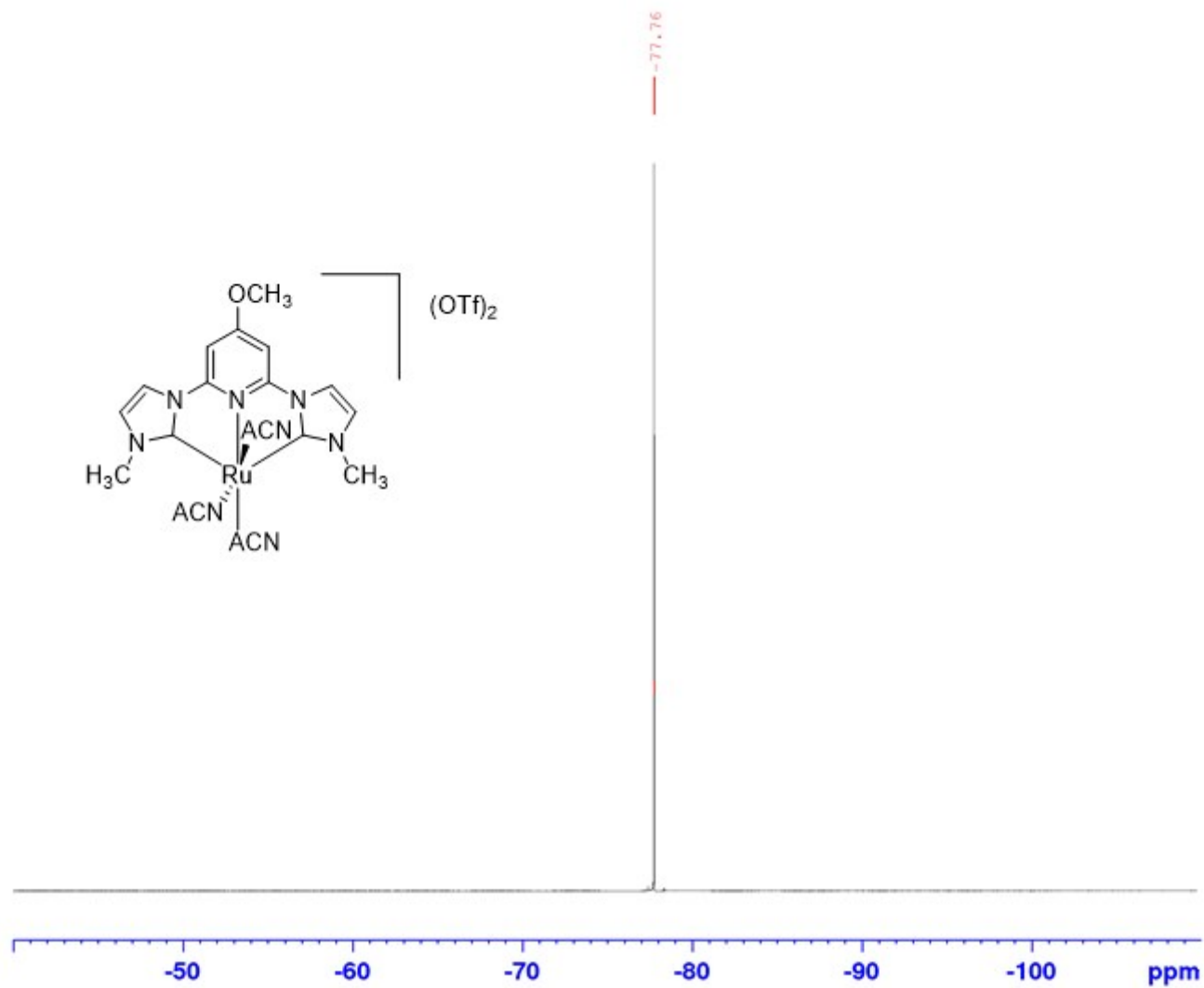


Figure S19: ^{19}F -NMR (339 MHz) of $[\text{Ru}(\text{CNC-OMe})(\text{ACN})_3](\text{OTf})_2$ (**3**) in DMSO.

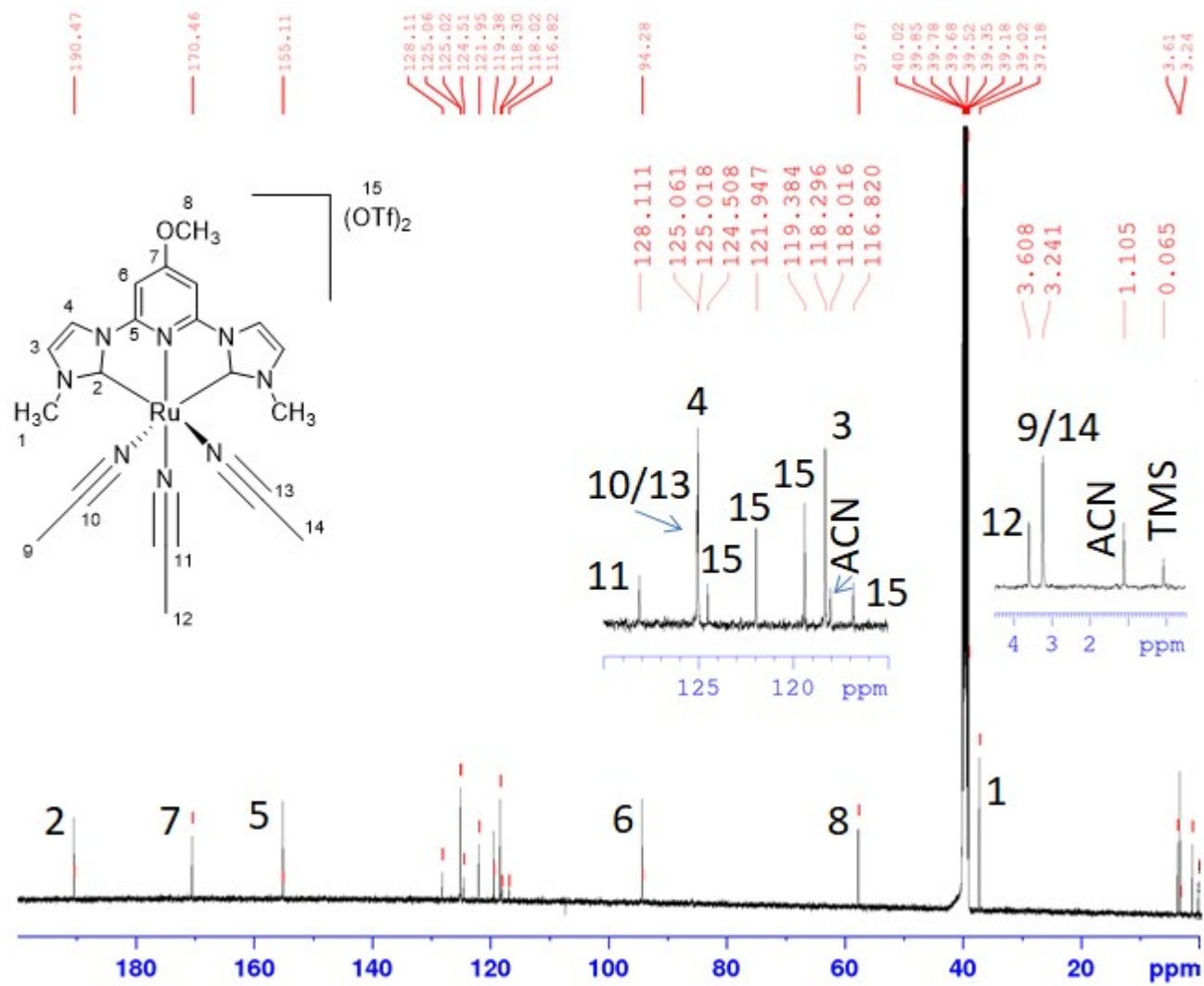


Figure S20: ^{13}C -NMR (126 MHz) of $[\text{Ru}(\text{CNC-OMe})(\text{ACN})_3](\text{OTf})_2$ (**3**) in DMSO.

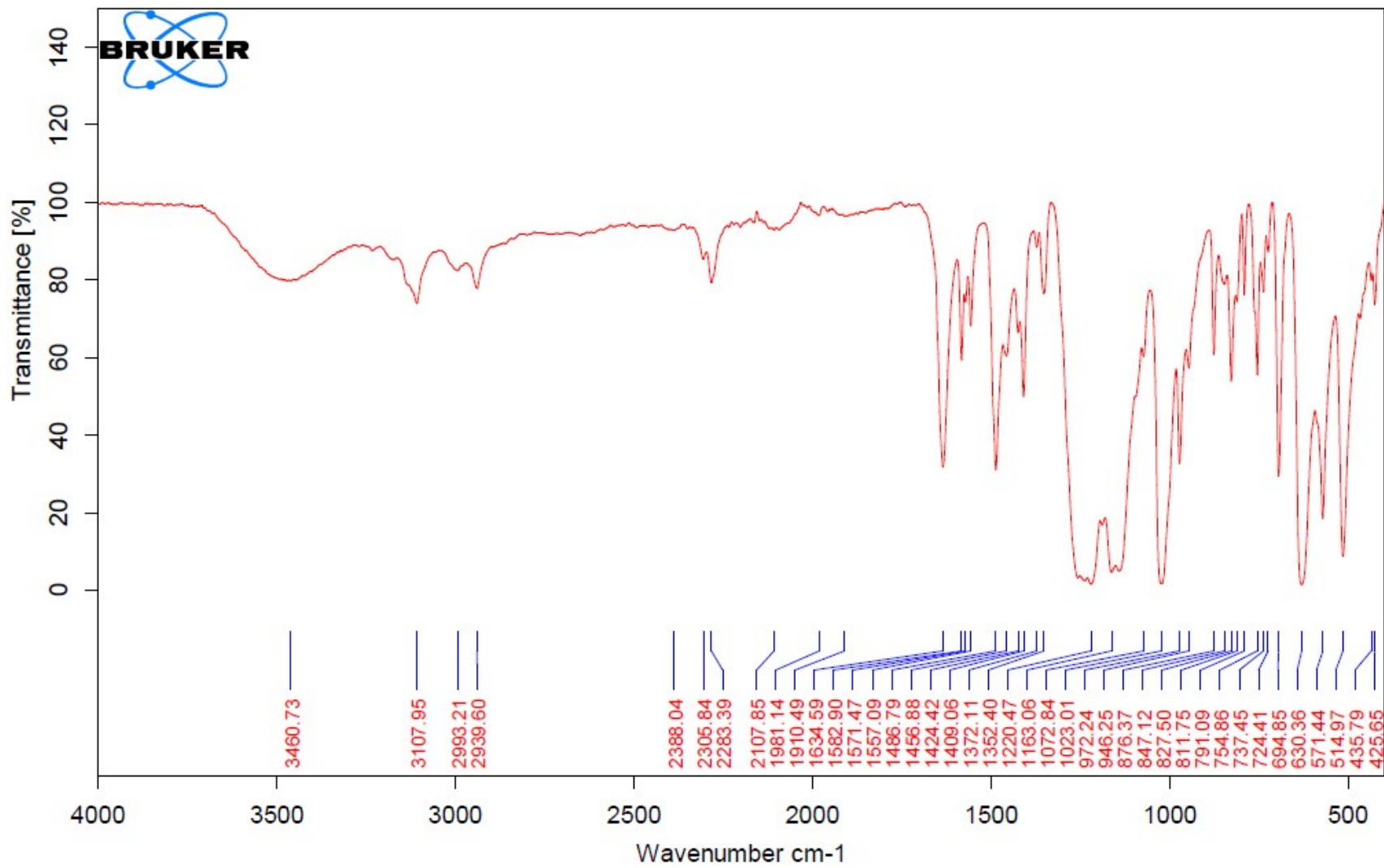


Figure S21: FT-IR (ATR) of $[\text{Ru}(\text{CNC-OMe})(\text{ACN})_3](\text{OTf})_2$ (**3**), neat.

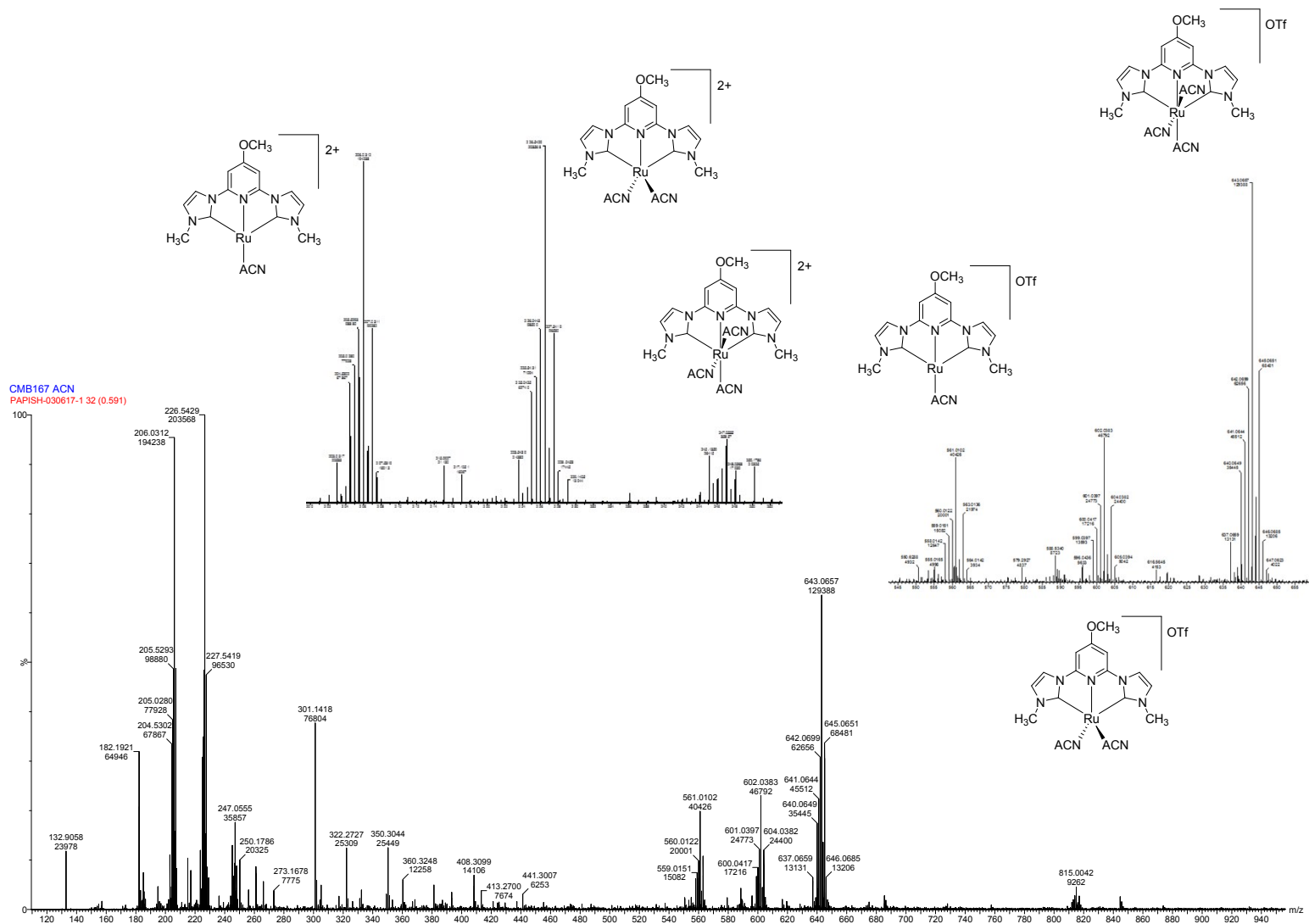


Figure S22: ESI-MS (ESI⁺) of [Ru(CNC-OMe)(ACN)₃](OTf)₂ (**3**).

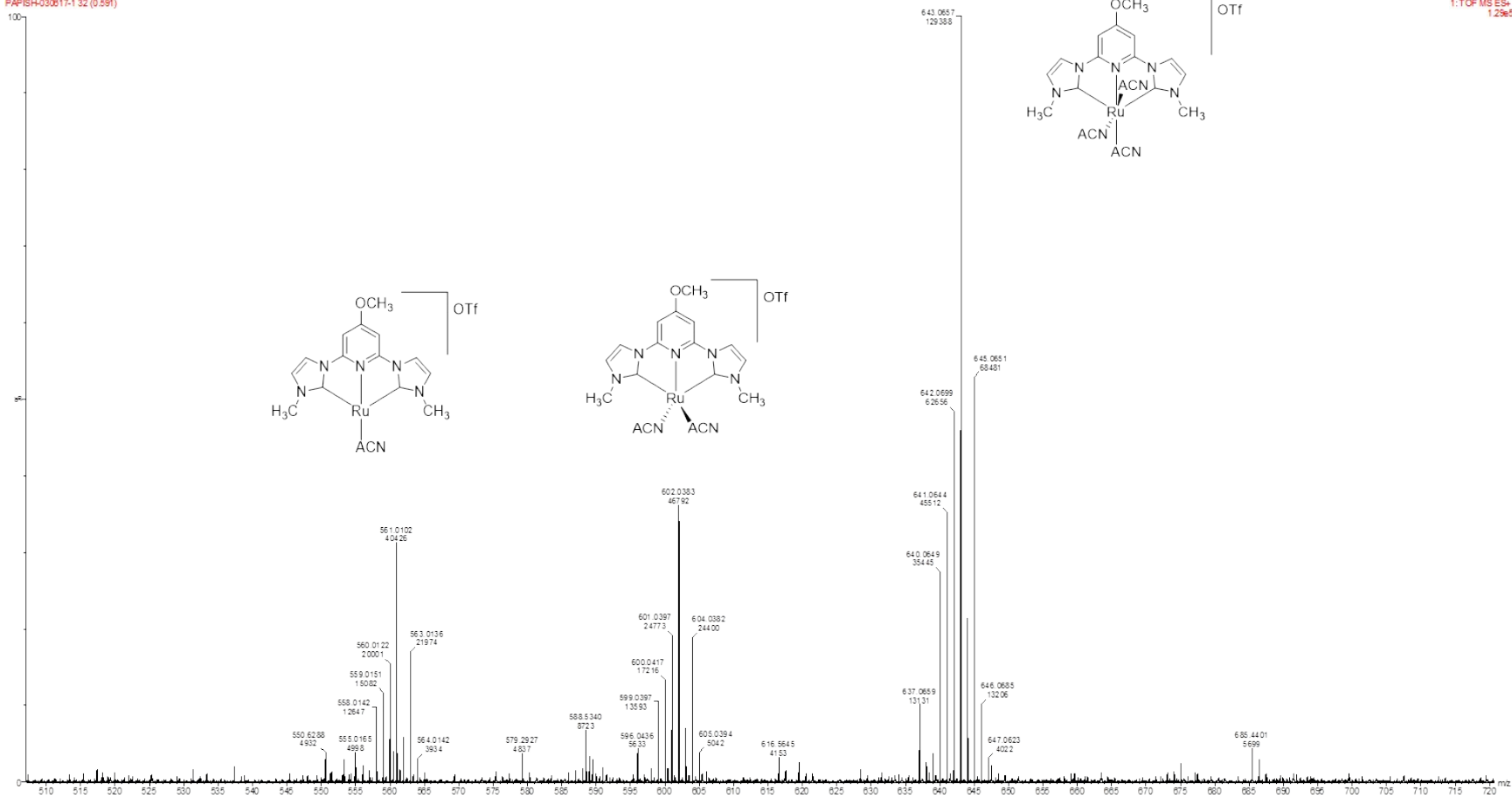


Figure S23: ESI-MS (ESI⁺) of $[\text{Ru}(\text{CNC-OMe})(\text{ACN})_3](\text{OTf})_2$ (**3**).

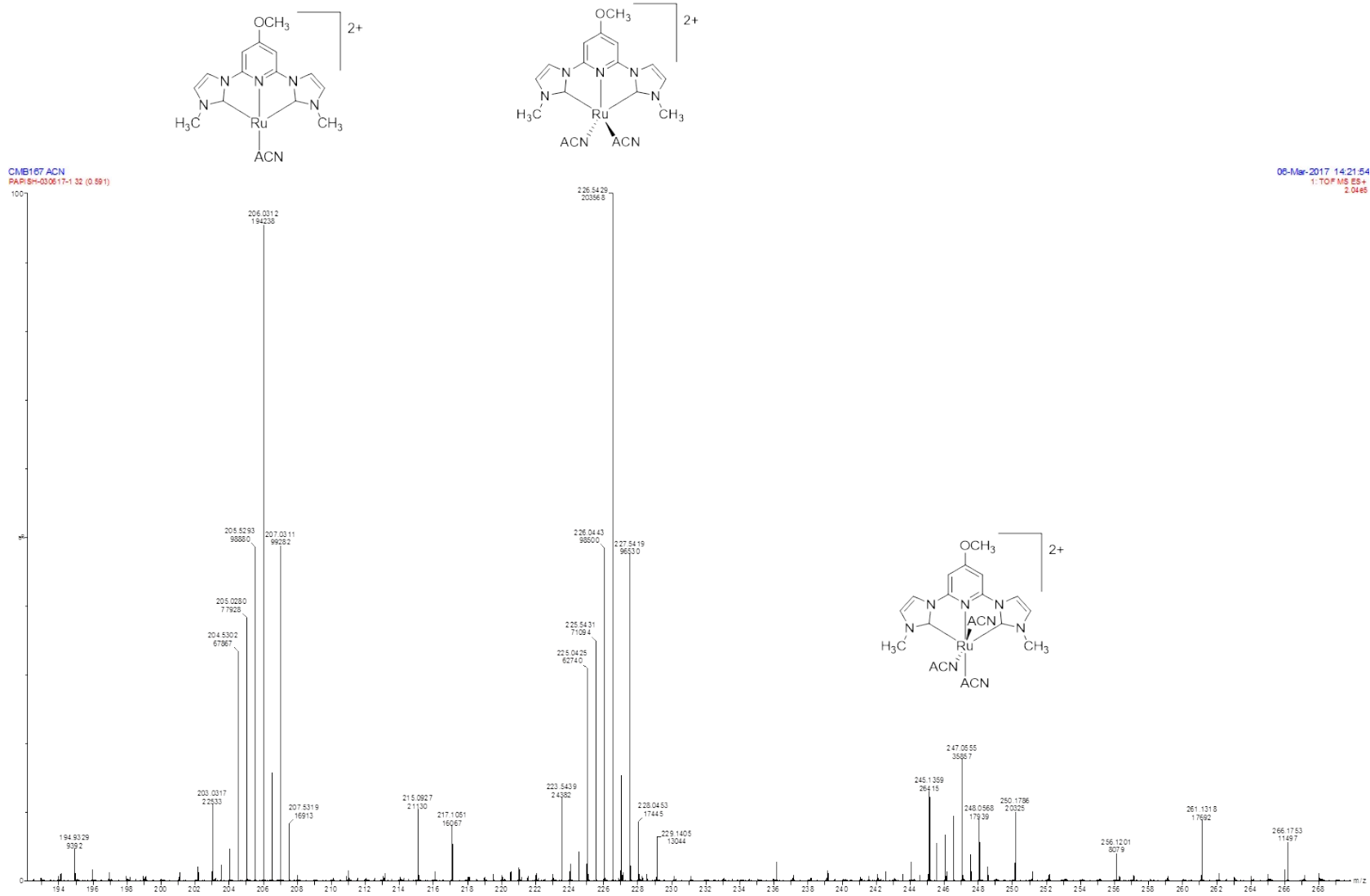


Figure S24: ESI-MS (ESI⁺) of [Ru(CNC-OMe)(ACN)₃](OTf)₂ (**3**).

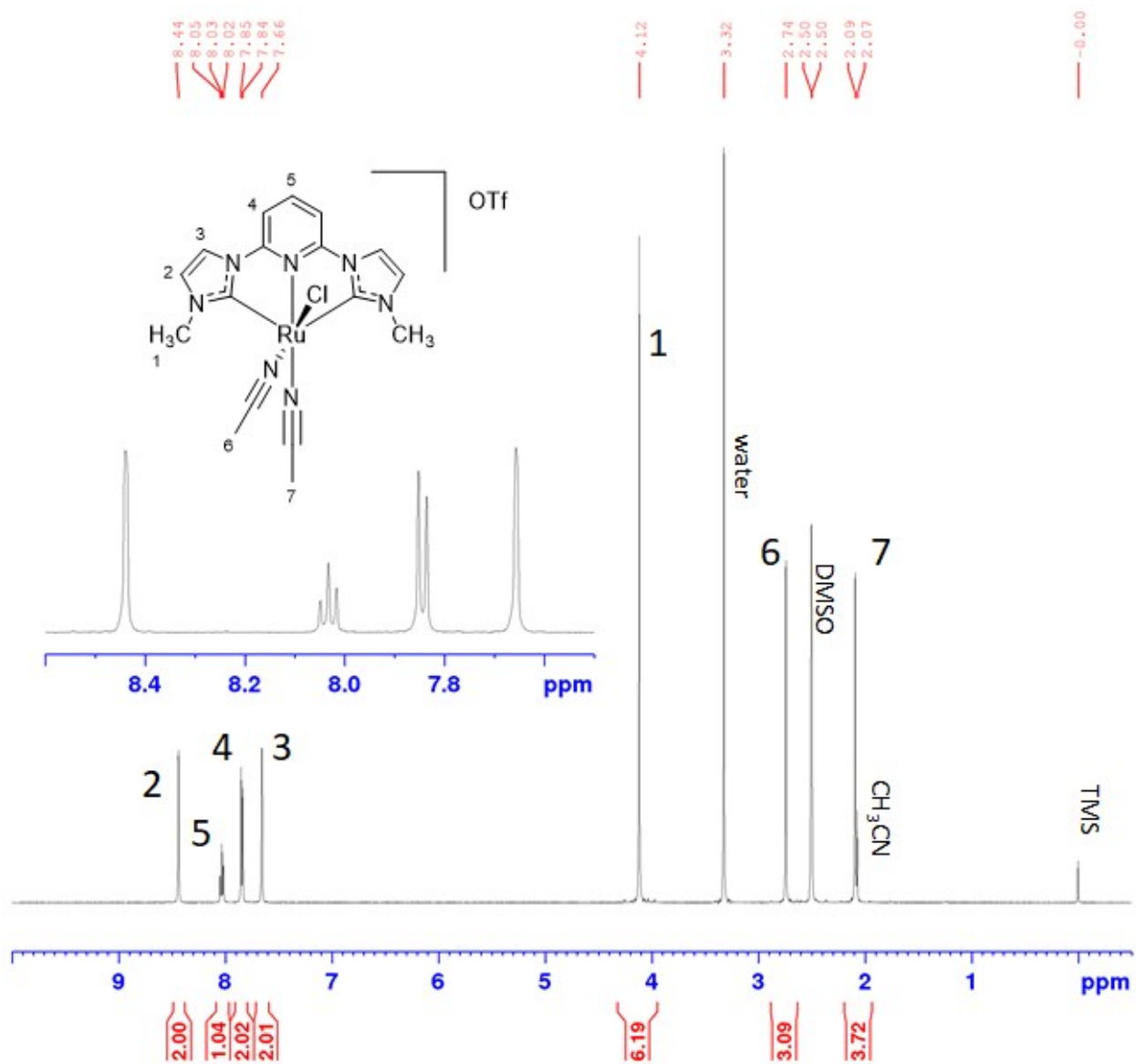


Figure S25: ¹H-NMR (360 MHz) of [Ru(CNC-H)(ACN)₂Cl]OTf (4) in DMSO.

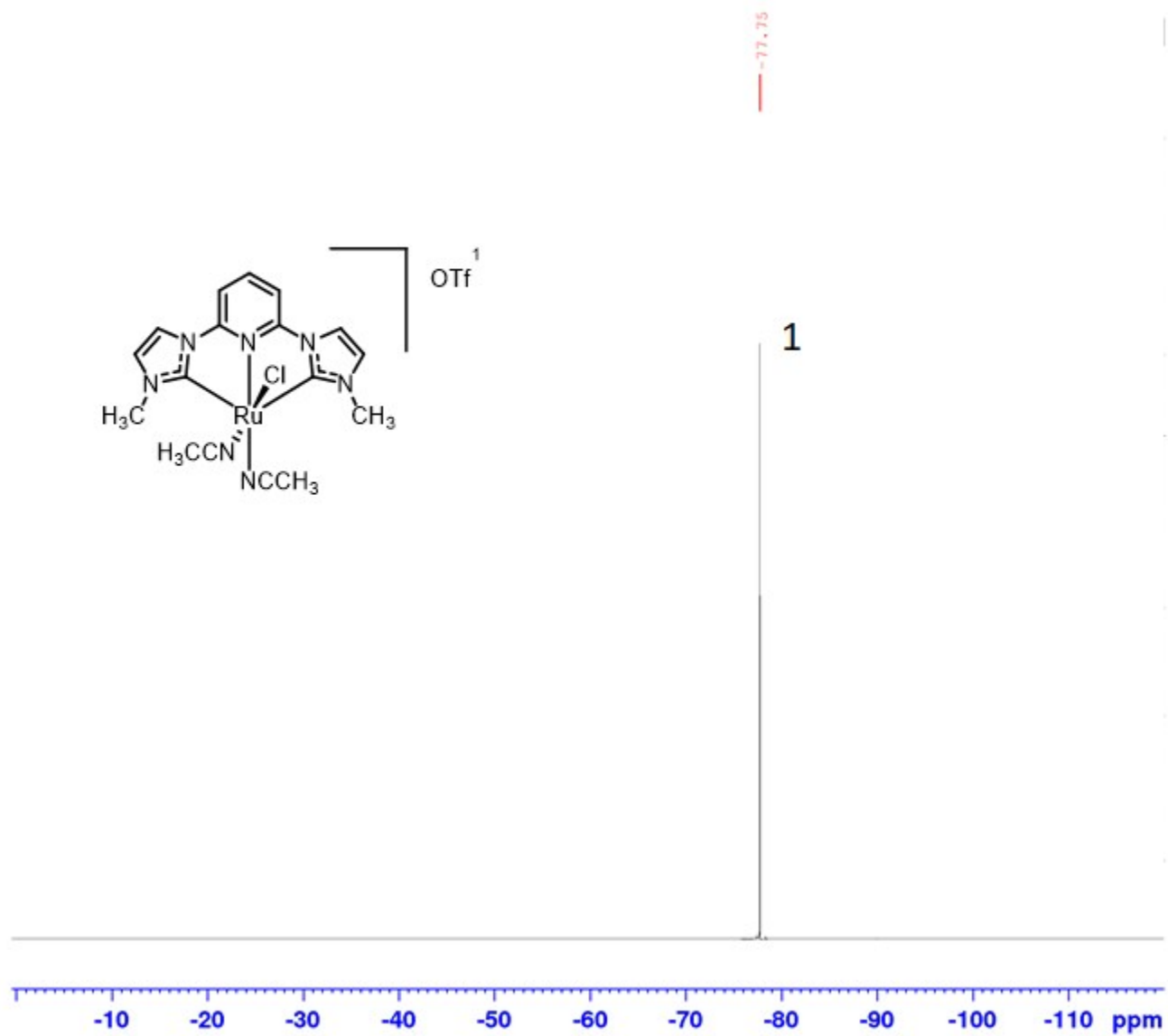


Figure S26: ^{19}F -NMR (339 MHz) of $[\text{Ru}(\text{CNC-H})(\text{ACN})_2\text{Cl}]\text{OTf}$ (4) in DMSO.

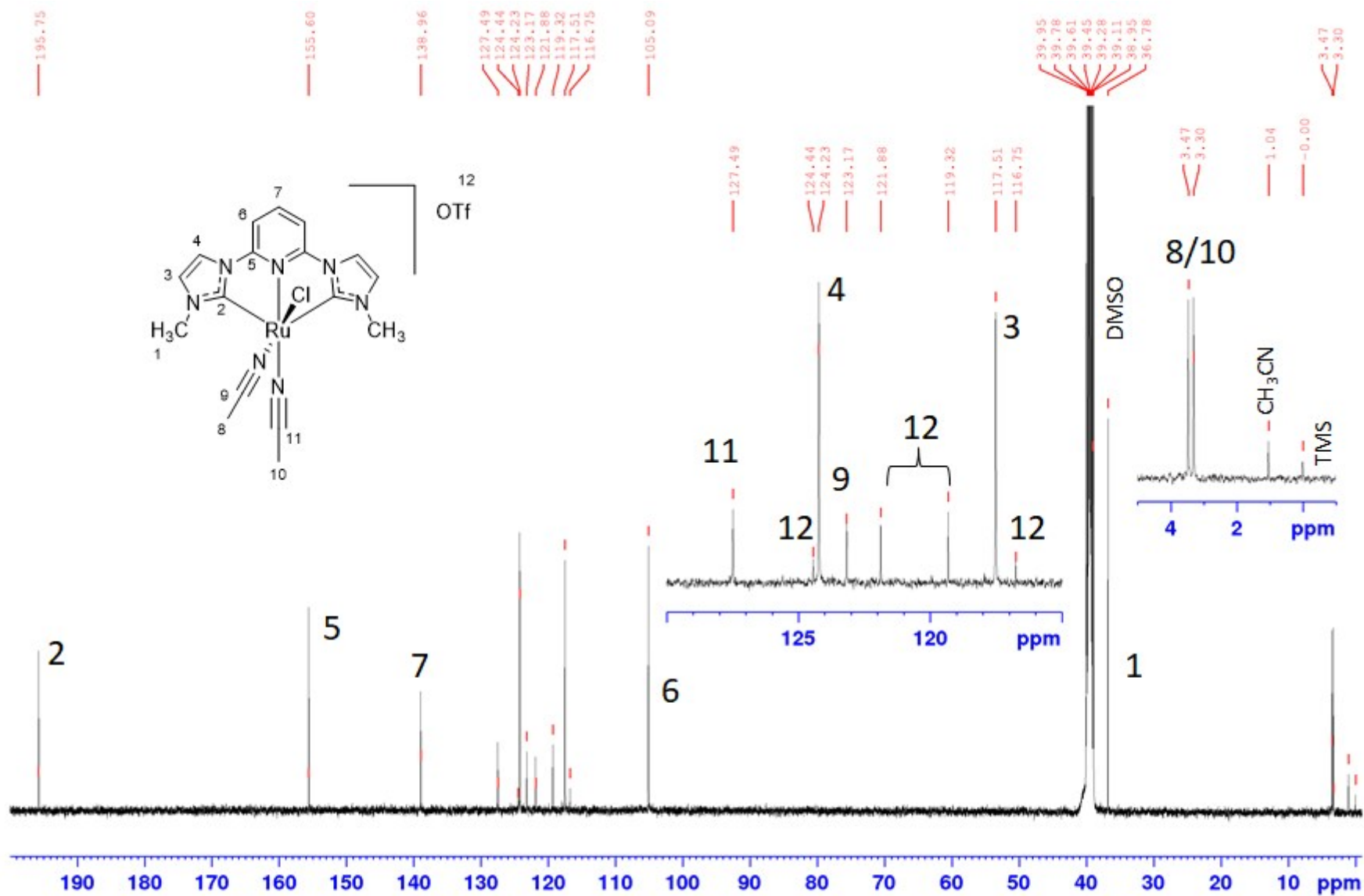


Figure S27: ^{13}C -NMR (126 MHz) of $[Ru(CNC-OMe)(ACN)_2Cl]OTf$ (**4**) in DMSO.

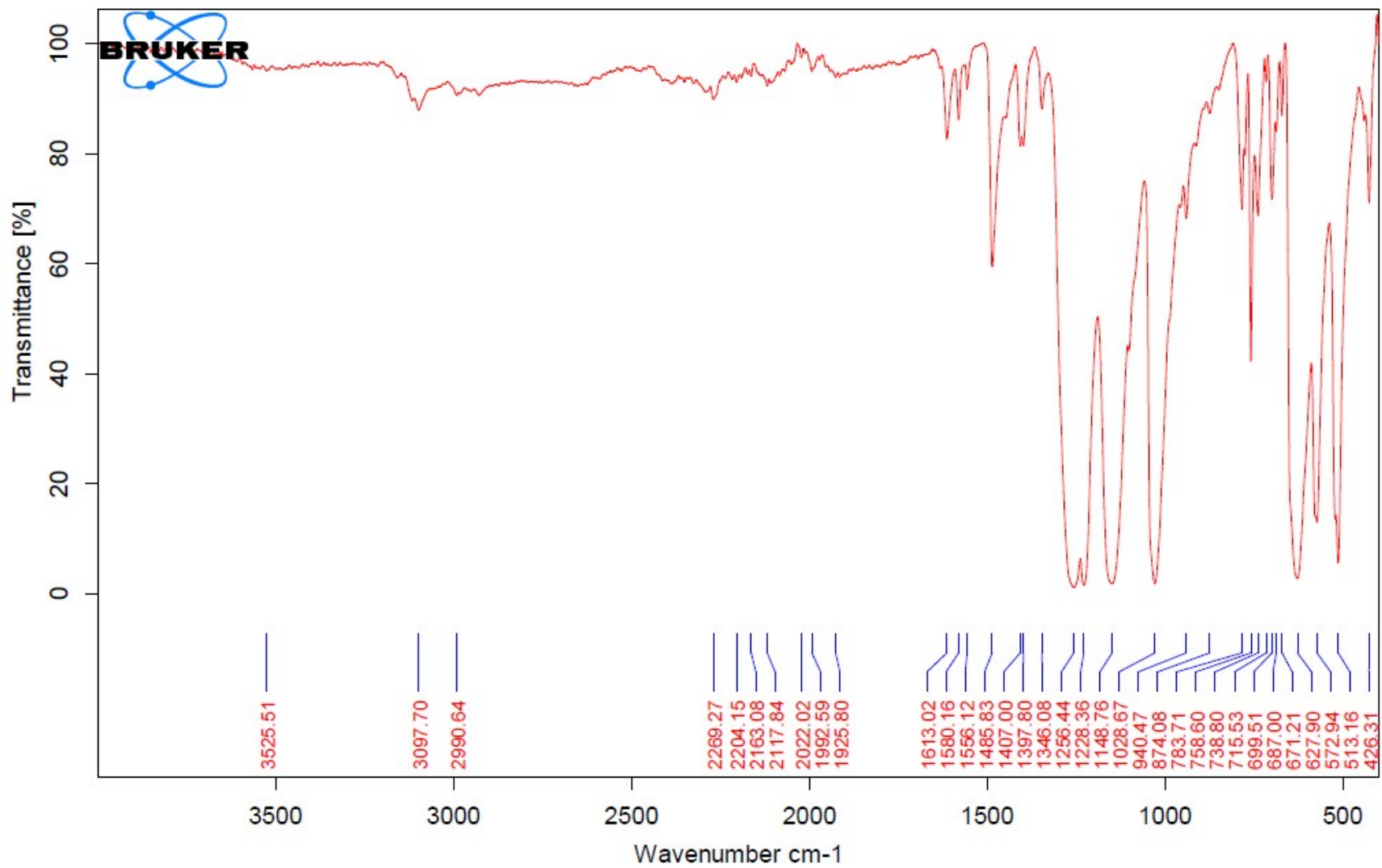


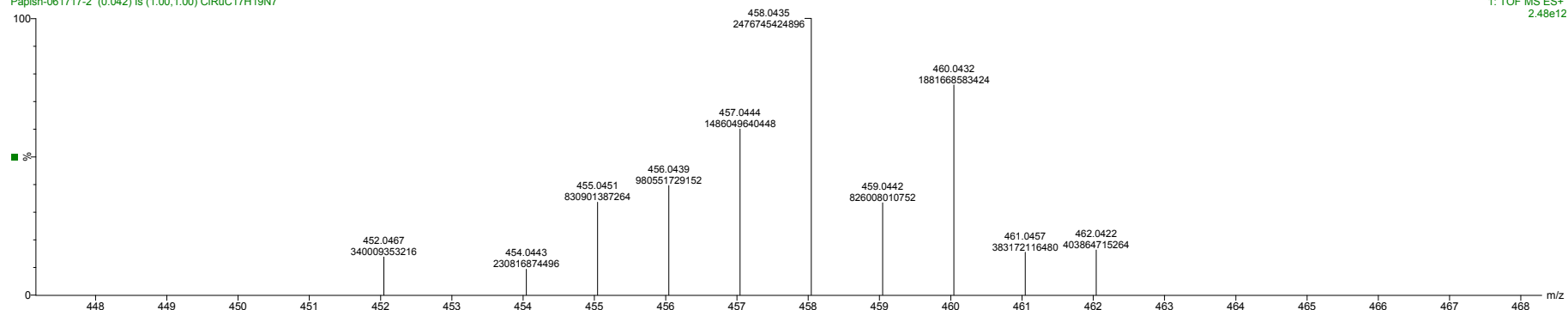
Figure S28: FT-IR (ATR) of [Ru(CNC-H)(ACN)₂Cl]OTf (**4**), neat.

INFUSION-CMB-192

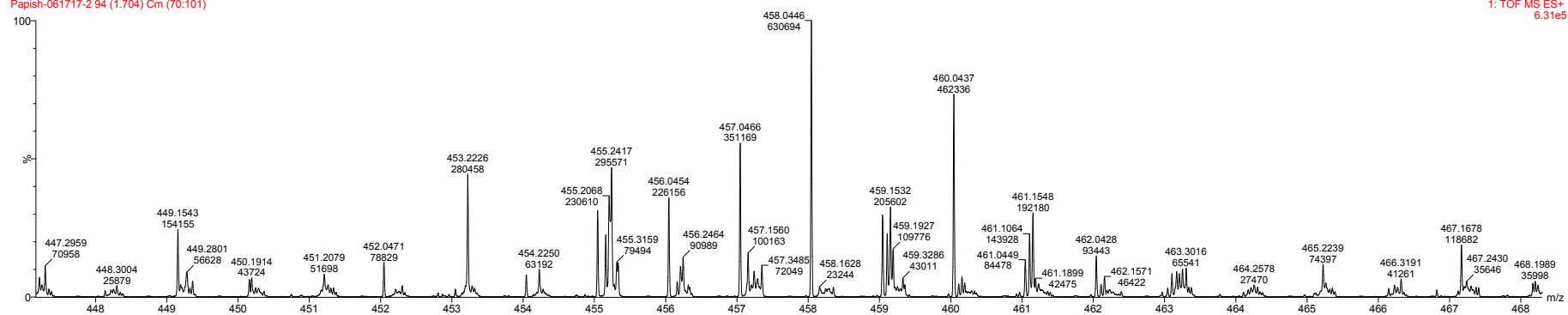
Papish-061717-2 (0.042) Is (1.00,1.00) ClRuC17H19N7

19-Jun-2017 15:30:50

1: TOF MS ES+
2.48e12



Papish-061717-2 94 (1.704) Cm (70:101)



1: TOF MS ES+
6.31e5

Figure S29: ESI-MS (ESI⁺) of [Ru(CNC-H)(ACN)₂Cl]OTf (4).

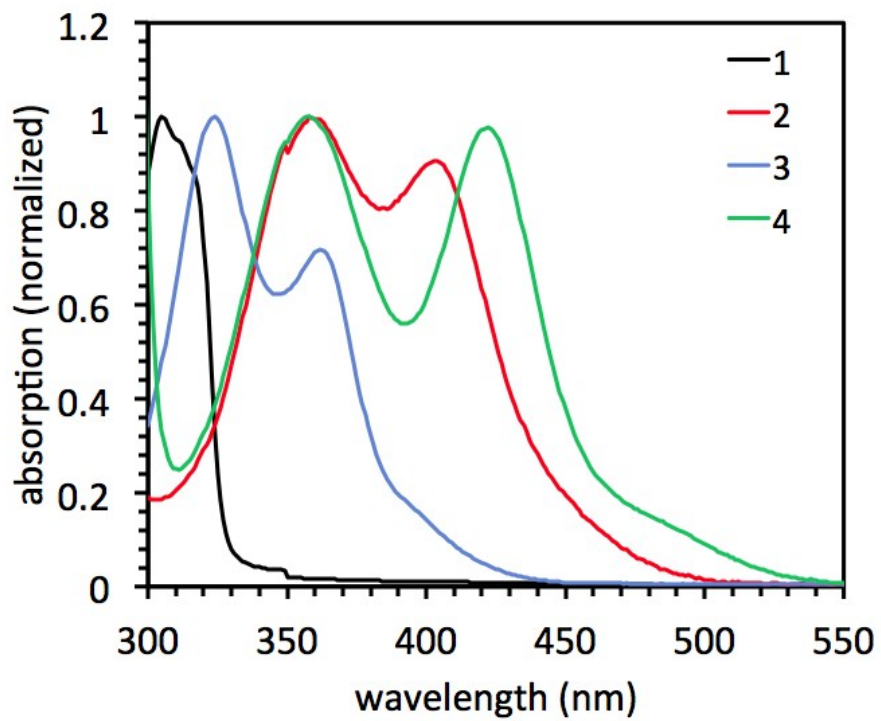


Figure S30: UV-Vis spectra for the catalysts in acetonitrile.

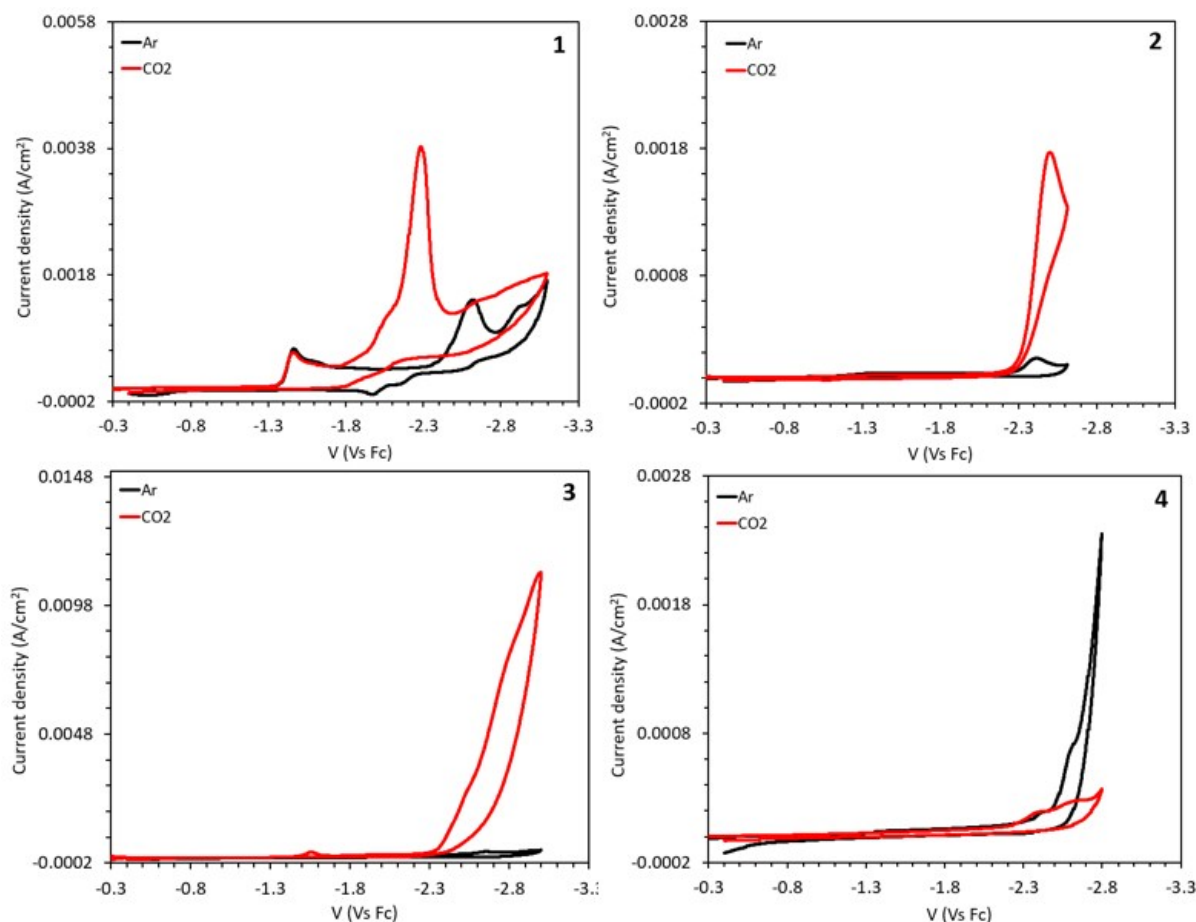


Figure S31: CVs of catalysts 1-4 in MeCN under with 1mM catalyst and 0.1 M n-Bu₄NPF₆ electrolyte under Ar (black) and CO₂ (red) atmosphere. Glassy carbon working electrode, platinum counter electrode, and Ag/AgCl reference electrodes are used for the measurements with a scan rate of 100 mV/s. All potential values are reported versus Fc/Fc⁺.

Thermodynamic Figure Discussion: Defining an overpotential in photocatalysis is exceptionally challenging. The standard reduction potential of CO₂ to CO is dependent on the lowest pK_a in solution, which is dynamic during photocatalysis. Establishing an overpotential for photocatalysis is not nearly as trivial as it is for electrocatalysis for several reasons: 1) sacrificial donors are acids post electron transfer which have challenging pK_a to define. For us the pK_a of the radical cation of BIH and the pK_a of the radical cation of TEA would have to be defined in MeCN. See our prior work for a brief description of what these are estimated to be: *Inorg Chem* 2016, 55, 682. Due to this we report the standard reduction potential range for CO₂ depending on what the lowest pK_a is in solution also taking into account carbonic acid if advantageous water is present. 2) The ionic strength of a solution can dramatically shift catalytic reduction potentials and the onset of CO₂ reduction catalysis is heavily dependent on the ions present. For these reasons, we are cautious to supply a suggested overpotential for each catalyst, which may be misleading, as electrocatalysis is typically done in a 1 M salt solution and photocatalysis does not incorporate such salts.

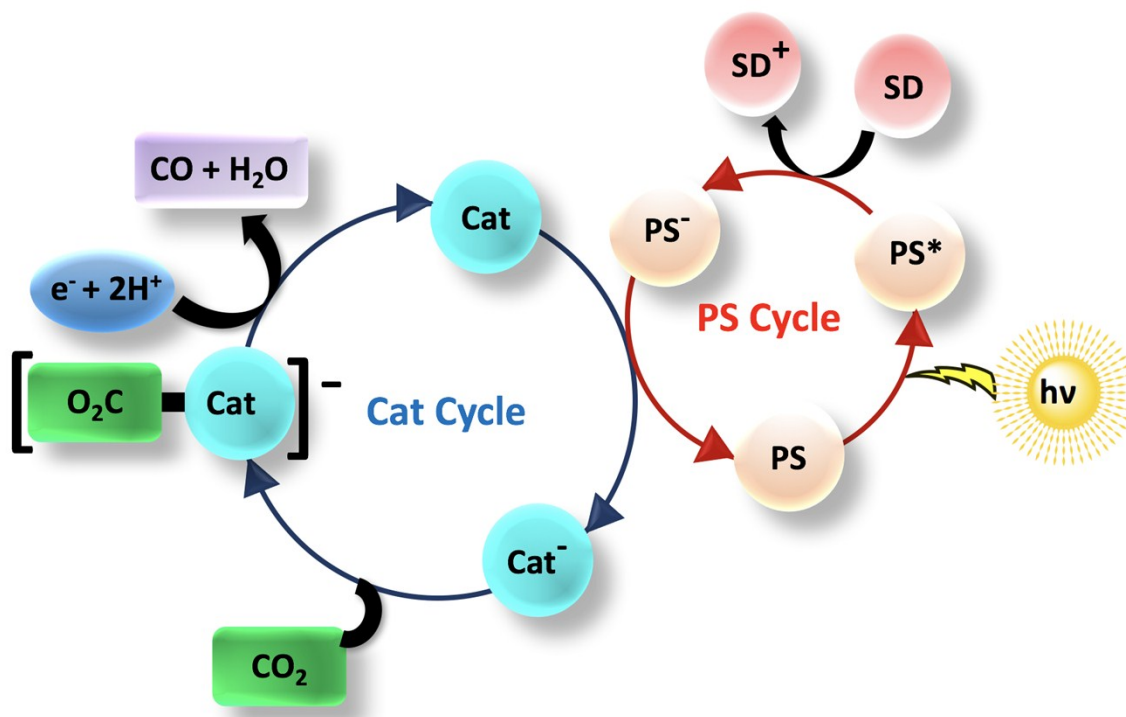


Figure S32: An illustration of a photocatalytic CO₂ reduction. **PS** is photosensitizer, **SD** is sacrificial donor, and **Cat** is catalyst

¹H NMR Formate Detection. Our slightly modified procedure is as follows: Upon reaction completion, 0.8 mL of the reaction solution was taken into a syringe and added to a 4 mL vial. To this 36 μ L of Verkade's Triisobutyl Superbase (CAS# 331465-71-5; 2,8,9-Triisobutyl-2,5,8,9-tetraaza-1-phosphabicyclo[3.3.3]undecane) or 36 μ L of DBU (1,8-Diazabicyclo[5.4.0]undec-7-ene) was added to the solution. If DBU is used, the sample solution is degassed with N₂ for 10 minutes and then refilled with MeCN to replace the original volume before adding DBU. This is necessary as DBU reacts with CO₂ and form a precipitate. This precaution is not necessary if using Verkade's Base. The mixture was sonicated for 10 minutes at room temperature. 1.16 mL of a d₃-MeCN ferrocene solution (1.19 mM concentration) was added to the mixture. The vial was thoroughly mixed, then an NMR spectrum was taken on a 500 MHz NMR or 300 MHz NMR with an extended D1-delay of 10 seconds and a minimum of 200 scans. The ratio of the formate peak (~8.7 ppm) and the ferrocene peak (~4.2 ppm, see below) were then compared to a calibration curve generated through the analysis of known concentrations of formate (0.0 mM, 0.1 mM, 1.0 mM, and 10.0 mM solutions). Through this

method the concentration of formate could be evaluated accurately through a trendline having an R^2 value of 0.997 and 0.999 (see below). All NMR spectra were evaluated with MestReNova software to ensure level baselines in the analyte region prior to integrating peaks.

Previously described here: Fei, H.; Sampson, M. D.; Lee, Y.; Kubiak, C. P.; Cohen, S. M. *Inorg. Chem.* **2015**, *54*, 6821.

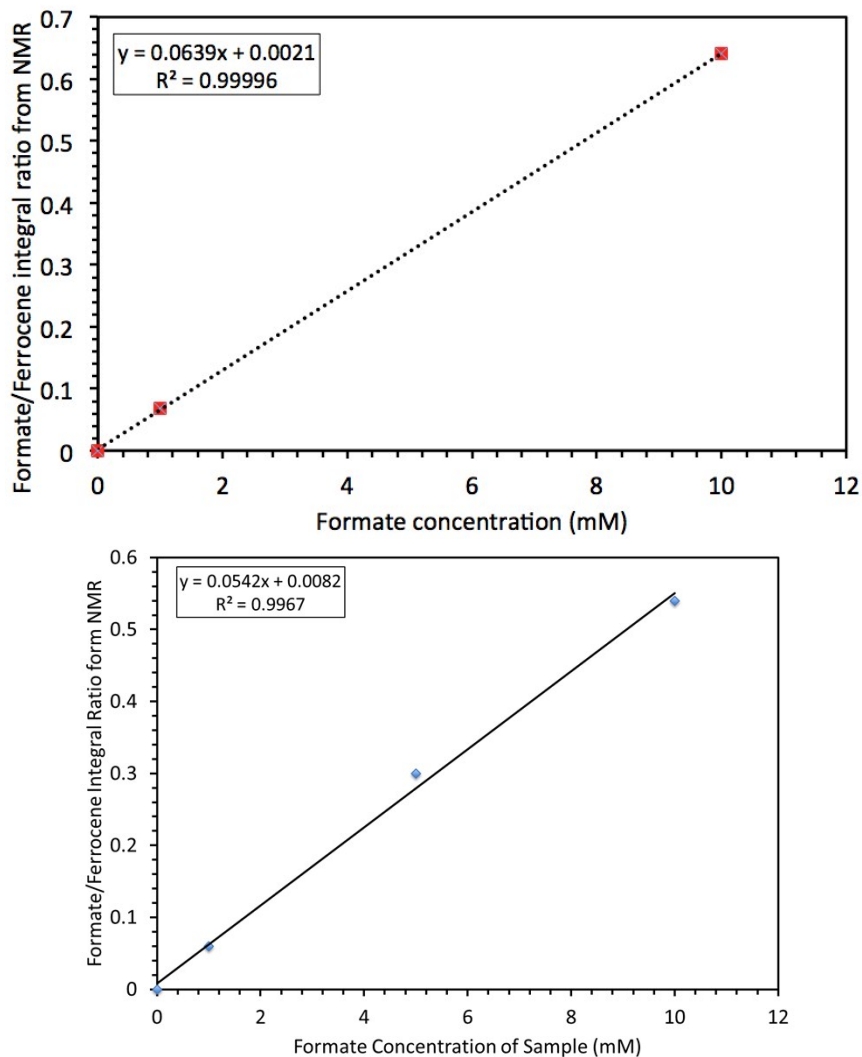


Figure S33: NMR formate calibration curve in d_3 -MeCN with ferrocene as an internal standard for DBU (left) and Verkade's base (right).

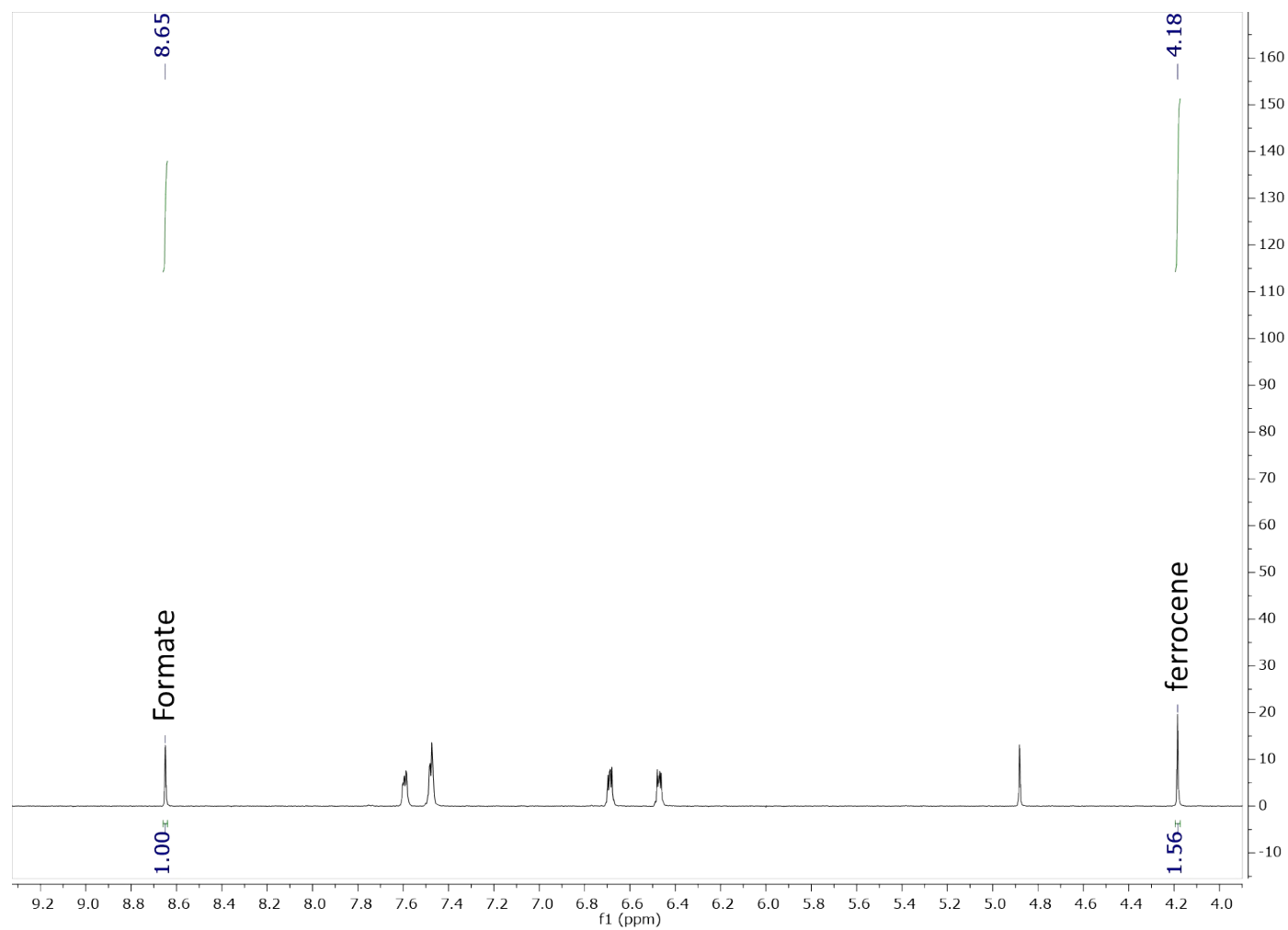


Figure S34: ¹H-NMR of formate in the presence of ferrocene as the internal standard and DBU as the base. This NMR is from a sample for the calibration curve above. No formate was observed for any catalyst in this study using our standard photocatalysis conditions listed above.

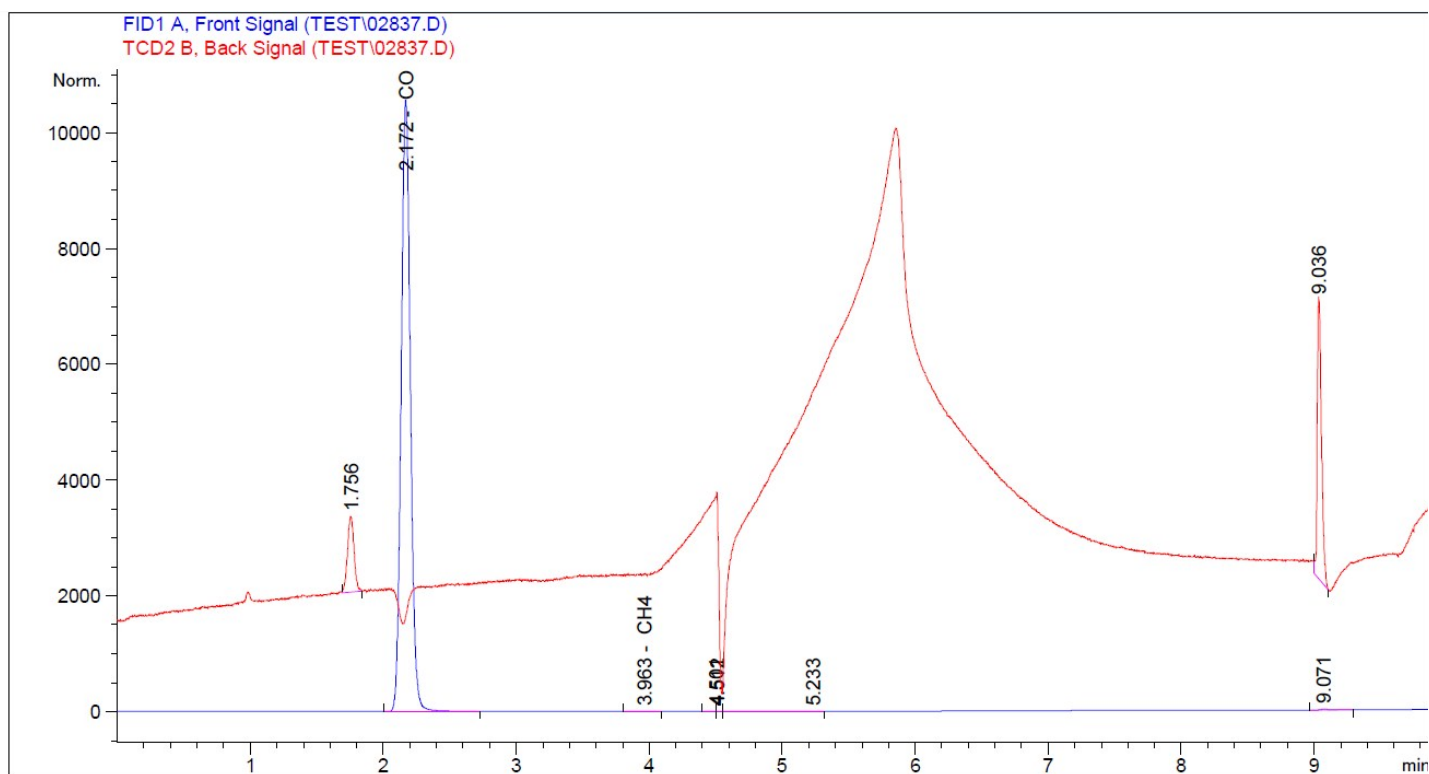


Figure S35: Example GC-trace for Ru photocatalytic reaction. FID detector is the blue trace and can detect CO and CH₄. Only CO is observed. The red trace is the TCD curve which can detect H₂ at ~1.0 minutes (not observed in substantial quantities). The TCD curve shows peak only as noise in the GC spectrum from the heat ramp cycle, backflush, and trace O₂. The y-axis is for the FID curve.

Table S1: Reaction conditions and products observed for the photocatalytic reduction of CO₂ with ruthenium complexes.

Catalyst (see images below table)	photosensitizer	proton/electron source	photon source	solvent	CO (TON)	HCO ₂ ⁻ (TON)	CO + HCO ₂ ⁻ (TON)	selectivity
non-photosensitized								
Ru(Me ₂ bpy) ₃ ⁱ	none	TEOA, BNAH	480 nm	DMF	3	25	28	89% HCO ₂ ⁻
Ru(Me ₂ bpy) ₃ ⁱ	none	TEOA, BNAH	480 nm	MeCN	2	14	16	88% HCO ₂ ⁻
Ru(phen) ₃ ⁱⁱ	none	AA, pyridine, KCl	LED	H ₂ O	0	76	76	100% HCO ₂ ⁻
intramolecular photosensitized								
Ru ^{cat} ₁ Ru ^{PS} ₂ ⁱⁱⁱ	covalently bound	TEOA, BNAH-OMe	500 W Xe	DMF	0	671	671	100% HCO ₂ ⁻
Ru ^{cat} ₁ Ru ^{PS} ₁ ⁱⁱⁱ	covalently bound	TEOA, BNAH	500 W Xe	DMF	13	315	328	96% HCO ₂ ⁻
Ru ^{cat} ₂ Ru ^{PS} ₁ ⁱⁱⁱ	covalently bound	TEOA, BNAH	500 W Xe	DMF	315	353	668	53% HCO ₂ ⁻
Ru ^{cat} ₃ Ru ^{PS} ₁ ⁱⁱⁱ	covalently bound	TEOA, BNAH	500 W Xe	DMF	358	234	592	60% CO
intermolecular photosensitized								
Ru(Me ₂ bpy) ₂ (CO) ₂ ⁱⁱⁱ	Ru(Me ₂ bpy) ₃	TEOA, BNAH	500 W Xe	DMF	113	316	429	74% HCO ₂ ⁻
Ru(bpy) ₂ (CO) ₂ ^{iv} complex 1, benchmark	Ru(bpy) ₃	BNAH, H ₂ O	300 W Hg	DMF	120	158	278	57% HCO ₂ ⁻
Ru(bpy)₂(CO)₂ complex 1, benchmark	Ru(bpy)₃	BNAH, H₂O	AM 1.5G solar simulator	DMF	20	126	146	86% HCO₂⁻
Ru(bpy)₂(CO)₂ complex 1, benchmark	Ir(ppy)₃	BIH, TEA	AM 1.5G solar simulator	MeCN	74	0	74	100% CO
(^{OMe}CNC)RuCl (complex 2)	Ir(ppy)₃	BIH, TEA	AM 1.5G solar simulator	MeCN	250	0	250	100% CO
(^{OMe}CNC)RuMeCN (complex 3)	Ir(ppy)₃	BIH, TEA	AM 1.5G solar simulator	MeCN	147	0	147	100% CO
(^HCNC)RuCl (complex 4)	Ir(ppy)₃	BIH, TEA	AM 1.5G solar simulator	MeCN	3	0	3	100% CO

[Table references: i.) Takeda, H.; Koizumi, H.; Okamoto, K.; Ishitani, O. Chem Commun, **2014**, 50, 1491-1493. li.) Boston, D. J.; Xu, C.; Armstrong, D. W.; MacDonnel, F. M. J. Am. Chem. Soc. **2013**, 135, 16252–16255 iii.) Tamaki, Y.; Morimoto, T.; Koike, K.; Isitani, O. PNAS. **2012**, 109, 15673-15678 v.) [Ishida, H.](#); [Terada, t.](#); [Tanaka, k.](#); [Tanaka, T.](#) *Inorganic. Chem.* **1990**, 29, 905-911]

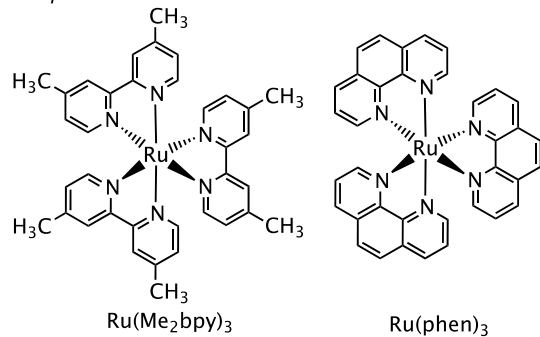
We note it is exceptionally difficult to compare TON numbers directly between catalyst systems which are not identical due to several factors including: 1) tremendously varied light intensities and wavelengths are frequently used ranging from low intensity light to potentially higher than 1 sun intensity depending on the distance from the lamp, 2) changes in lamp intensities over time require careful calibrations to manage photon intensities which often leads to difficulty comparing results with the same lamp in terms of wattage if the power is not reported, 3) the use of non-innocent photosensitizers such as Ru(Me₂bpy)₃ which are themselves photocatalysts but are not calculated in the

TON equation, and 4) variable solvent conditions allowing variable proton and electron sources, some of which have been confirmed generators of CO or HCO₂⁻.

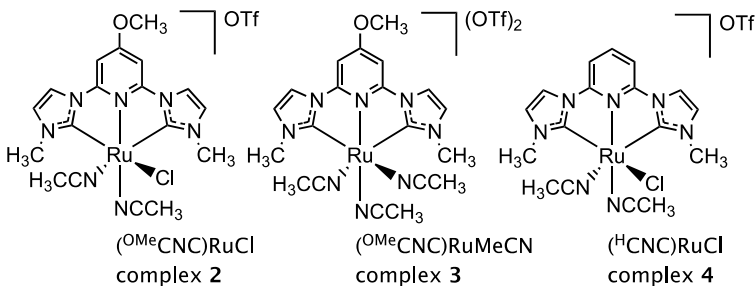
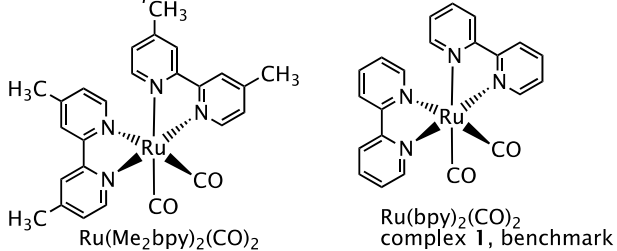
The variable light source intensity is particularly concerning as this is known to have large effects on durability and initial rates. For this reason, we have chosen to synthesize a benchmark catalyst (Ru(bpy)₂(CO)₂, complex 1) and compare it directly to the Ru(CNC-pincer) catalysts [(^{OMe}CNC)RuCl (complex 2), (^{OMe}CNC)RuMeCN (complex 3), (^HCNC)RuCl (complex 4)] under a 1 sun calibrated lamp (AM 1.5G) with an inert photosensitizer in a solvent/donor system with no background product production to standardize our lab's measurements for future comparisons. Directly comparing bottom line TON numbers in literature with tremendously varied conditions should be pursued with extreme caution. **As an example of this, the identical catalyst Ru(bpy)₂(CO)₂ (complex 1) gives a non-selective 278 total TON with a 300 W Hg lamp/BNAH/H₂O/DMF/Ru(bpy)₃ system, 146 total TON with an AM 1.5G solar simulator/BNAH/H₂O/DMF/Ru(bpy)₃ system and 74 TON with an AM1.5G solar simulator/BIH/TEA/MeCN/Ir(ppy)₃ in the table above.**

An additional word of caution in comparisons within the above table: non-photosensitized, intermolecular photosensitized and intramolecular photosensitized systems should be independently compared given the dramatic differences in complexity and the large differences in performance of the three categories.

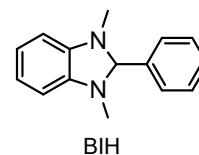
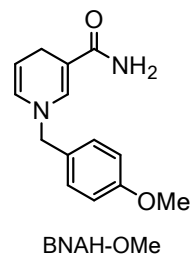
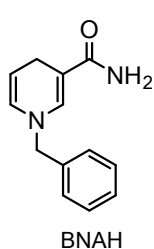
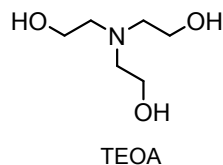
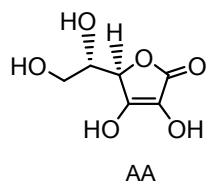
non-photosensitized



intermolecular photosensitized



Sacrificial Electron and Proton Source



intramolecular photosensitized

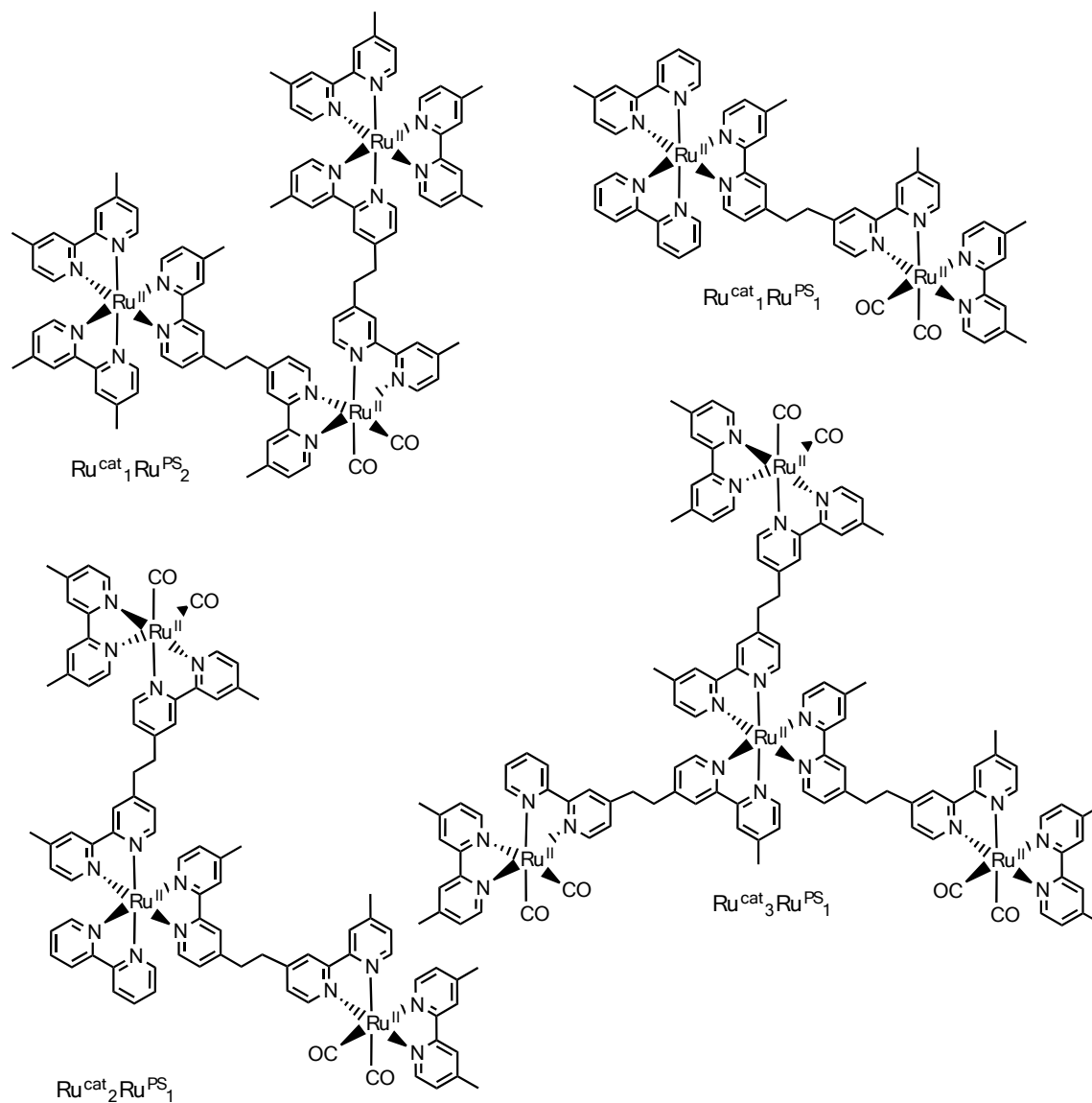


Figure S36: Structures of known Ru catalysts for Photocatalytic CO₂ reduction and sacrificial electron and proton sources.

XRD Structure Determination. A crystal of appropriate dimension was mounted on Mitegen cryoloops in a random orientation. Preliminary examination and data collection were performed on a Bruker Apex2 CCD-based X-ray diffractometer³ equipped with an Oxford N-Helix Cryosystem low temperature and a fine focus Mo-target X-ray tube ($\lambda = 0.71073 \text{ \AA}$) operated at 2000 W power (50 kV, 40 mA). The X-ray intensities were measured at 223 (2) K. The collected frames were integrated with the Saint⁴ software using a narrow-frame algorithm. Data were corrected for absorption effects using the multi-scan method in SADABS. The space groups were assigned using XPREP of the Bruker ShelXTL⁵ package, solved with ShelXT⁵ and refined with ShelXL⁵ and the graphical interface ShelXle⁶. All non-hydrogen atoms were refined anisotropically. H atoms attached to carbon were positioned geometrically and constrained to ride on their parent atoms. Specific structure determination details are included in Table S1.

The structure of **3** was found to have a triply occupationally disordered CF_3SO_3^- ligand. The three components integrate to a ratio of 0.463:0.325:0.211, with the major component nearly perpendicular to the other two minor components. The overall occupancy of the three components was restrained to be unity by the Shelxl command SUMP. The three moieties were further restrained to have similar geometries (SAME command of Shelxl).

These structures have been deposited in the Cambridge Structural Database with deposit numbers CCDC 1563864-1563865.

Table S2 – Selected metric parameters for crystal structures **2** and **3**.

	Complex 2	Complex 3
Crystal data		
Chemical formula	C ₂₁ H ₂₄ ClF ₃ N ₈ O ₄ RuS	C ₂₂ H ₂₄ F ₆ N ₈ O ₇ RuS ₂
<i>M</i> _r	678.06	791.68
Space group	Monoclinic, <i>P</i> 2 ₁ / <i>c</i>	Triclinic, <i>P</i> -1
Temperature (K)	223 (2)	223 (2)
Unit cell dimensions	a = 14.4683 (5) Å b = 25.8841 (8) Å c = 7.7287 (2) Å α = 90° β = 103.616 (2)° γ = 90°	a = 7.9326 (14) Å b = 9.4243 (17) Å c = 20.804 (4) Å α = 97.577 (2)° β = 91.192 (2)° γ = 93.256 (2)°
<i>V</i> (Å ³)	2813.04 (15)	1538.6 (5)
<i>Z</i>	4	2
Radiation type	Mo <i>K</i> α	Mo <i>K</i> α
μ (mm ⁻¹)	0.789	0.74
Crystal size (mm)	0.20 × 0.18 × 0.07	0.13 × 0.09 × 0.03
Data collection		
Diffractometer	AXS SMARTAPEX2 CCD	AXS SMART APEX2 CCD
Absorption corr.	Multi-scan SADABS	Multi-scan SADABS
<i>T</i> _{min} , <i>T</i> _{max}	0.667, 0.746	0.689, 0.746
No. of measured, independent and observed [<i>I</i> > 2σ(<i>I</i>) reflections	46175 7893 6719	41923 7621 6551
<i>R</i> _{int}	0.029	0.042
(sin θ/λ) _{max} (Å ⁻¹)	0.696	0.668
Refinement		
<i>R</i> [<i>F</i> ² > 2σ(<i>F</i> ²)]	0.028	0.041
<i>wR</i> (<i>F</i> ²)	0.071	0.116
<i>S</i>	1.04	1.10
No. of reflections	7893	7621
No. of parameters	358	568
No. of restraints	0	685
H-atom treatment	Constrained	constrained
Δρ _{max} , Δρ _{min} (e Å ⁻³)	0.56, -0.65	0.81, -0.65

References.

1. Winter, S. M.; Roberts, R. J.; Mailman, A.; Cvrkalj, K.; Assoud, A.; Oakley, R. T., Thermal conversion of a pyridine-bridged bisdithiazolyl radical to a zwitterionic bisdithiazolopyridone. *Chemical Communications* **2010**, *46* (25), 4496-4498.
2. Sheng, M.; Jiang, N.; Gustafson, S.; You, B.; Ess, D. H.; Sun, Y., A nickel complex with a biscarbene pincer-type ligand shows high electrocatalytic reduction of CO₂ over H₂O. *Dalton Transactions* **2015**, *44* (37), 16247-16250.
3. Bruker *Apex2*, Apex2 2013.10-0; Bruker AXS Inc.: Madison, Wisconsin, USA, 2007.
4. Bruker *Saint Plus*, Saint Plus 8.34A; Bruker AXS Inc.: Madison, Wisconsin, USA, 2007.
5. Sheldrick, G. M., SHELXTL v. 2008; ShelXT v. 2014/4 ; SHELXL v. 2014/7; Cell_Now. *Acta Cryst.* **2008**, *A64*, 112-122.
6. Hübschle, C. B.; Sheldrick, G. M.; Dittrich, B., ShelXle: a Qt graphical user interface for SHELXL. *J. Appl. Cryst.* **2011**, *44*, 1281-1284.